Lawrence Berkeley National Laboratory
Recent Work

Title
STRESS CORROSION CRACKING OF A TRIP STEEL

Permalink
https://escholarship.org/uc/item/3qr4096c

Author
Birat, Jean-Pierre.

Publication Date
1970-11-01

eScholarship.org Powered by the California Digital Library
University of California

RECEIVED
LAWRENCE
RADIATION LABORATORY

NOV 13 1970

LIBRARY AND
DOCUMENTS SECTION

UCRL-20300

c.2

STRESS CORROSION CRACKING OF A TRIP STEEL

Jean-Pierre Birat
(M. S. Thesis)

September 1970

AEC Contract No. W-7405-eng-48

TWO-WEEK LOAN COPY

This is a Library Circulating Copy which may be borrowed for two weeks. For a personal retention copy, call Tech. Info. Division, Ext. 5545

UCRL

LAWRENCE RADIATION LABORATORY
UNIVERSITY of CALIFORNIA BERKELEY

UCRL-20300

DISCLAIMER

This document was prepared as an account of work sponsored by the United States Government. While this document is believed to contain correct information, neither the United States Government nor any agency thereof, nor the Regents of the University of California, nor any of their employees, makes any warranty, express or implied, or assumes any legal responsibility for the accuracy, completeness, or usefulness of any information, apparatus, product, or process disclosed, or represents that its use would not infringe privately owned rights. Reference herein to any specific commercial product, process, or service by its trade name, trademark, manufacturer, or otherwise, does not necessarily constitute or imply its endorsement, recommendation, or favoring by the United States Government or any agency thereof, or the Regents of the University of California. The views and opinions of authors expressed herein do not necessarily state or reflect those of the United States Government or any agency thereof or the Regents of the University of California.

Contents

ABSTRACT ---------- v

LIST OF SYMBOLS ---------- vii

I. INTRODUCTION ---------- 1

II. MATERIAL STUDIED ---------- 5

III. EXPERIMENTAL PROCEDURE ---------- 7

A. Tensile Tests ---------- 7

B. Fracture Tests ---------- 7

C. Fatigue Tests ---------- 9

D. Fractography Observations ---------- 9

IV. RESULTS AND OBSERVATIONS ---------- 10

A. Tensile Tests ---------- 10

B. Toughness Tests ---------- 11

C. Fatigue Tests ---------- 12

1. Tests Results ---------- 12

2. Fractography ---------- 13

V. INTERPRETATION ---------- 15

A. Strain Rate Effect and TRIP Phenomenon ---------- 15

B. Water Effect and Hydrogen Embrittlement ---------- 18

C. Estimation of a Lower Value of the Fracture Toughness in the Case where no Value can be Measured ---------- 19

VI. CONCLUSIONS ---------- 21

ACKNOWLEDGMENTS ---------- 22

APPENDIX ---------- 23

REFERENCES ---------- 26

TABLES ---------- 29

FIGURE CAPTIONS ---------- 37

FIGURES ---------- 41

STRESS CORROSION CRACKING OF A TRIP STEEL

Jean-Pierre Birat

Inorganic Materials Research Division, Lawrence Radiation Laboratory
Department of Materials Science and Engineering, College of Engineering
University of California, Berkeley, California

ABSTRACT

Tensile, toughness and fatigue tests were conducted on a 0.27 C, 8 Ni, 12 Cr Metastable Austenitic Steel to test the effect of strain-rate and environment. Increasing the strain-rate was found to increase the yield-strength and the crack-growth rate in fatigue, to decrease the elongation and the tensile strength, and to allow a crack to become unstable in a constant strain-rate toughness-test. The effect of distilled water was found to bring down the toughness instability to strain-rates one-thousand times smaller than in air tests although all the values recorded were above 300 ksi/in.$^{1/2}$, to increase the crack growth rate in fatigue and to show delaminations in fracture surface observation by SEM. The TRIP phenomenon explained correctly the strain-rate effect and the assumption of hydrogen-embrittlement explained the water effect.

List of Symbols

a	Crack length
a_0	Initial crack length
B	Thickness of a specimen
C	Compliance
E	Young's modulus
G	Energy release rate per unit crack length
ΔG	Activation energy
K	Stress intensity factor (SIF). The subscripts I, II, III refer to fracture modes I, II, and III.
K_C	Fracture toughness
ΔK	Range of K in a fatigue test
M_S	Temperature at which martensite forms by quenching
M_D	Temperature at which martensite forms by quenching
M^*_{D30}	Temperature at which 30% deformation gives rise to 50% martensite in an annealed material
M_{D30}	Same as M^*_{D30} but for a worked material
n	Number of cycles
P	Load
R	Gas constant
r_y	Plastic zone radius
S	Cross-section area of a specimen
S_y	Yield strength

T	Absolute temperature
W	Width of specimen
x	Displacement
(x_m, P_m)	Coordinates of the maximum point in a load-displacement curve recorded in fracture testing of SEN specimens
δ	Deformation during processing of a TRIP Steel
θ	Temperature of the last hot rolling of a TRIP Steel
λ, μ	Proportionality functions
SEM	Scanning Electron Microscope
SEN	Single-edge-notched (specimen)
TRIP	TRansformation Induced Plasticity

I. INTRODUCTION

Metallurgy today is entering a transitional period in its historical evolution. Yesterday it was still an engineering art, existing through its craftmen's experience and progressing by timid attempts around empirically ascertained results. Tomorrow the designers will be entitled to ask it to produce at will a material with specified properties. Right now the field of metallurgy is earning a scientific status: from the fundamental and rather unrelated topics grouped together under its name, it begins to define the methods by which the program set forth for the future will be achieved.

Progressive industries furnish the most dynamic demand for new materials. The aeronautical industry for instance, asks for high strength and good resistance to fatigue, corrosion and high temperatures, with the additional condition that the yield strength to density ratio stays above a reasonable value, estimated at about 250,000 inches.

The research program being currently carried out in the Lawrence Radiation Laboratory under the influence of Professors Zackay and Parker stands at the forefront of this evolution. Fundamental reflections over the martensitic transformation have led to the algorithm of processing of the high strength metastable austenitic steels now known as TRIP steels, the characteristics of which we will now briefly review.

A martensitic transformation can be induced either by quenching or by straining, provided that the temperature is under definite values, respectively noted M_s and M_D.[1] In the case of the transition $\gamma \rightarrow \alpha'$ (austenite → martensite) in an alloyed steel, a careful selection of the chemical composition can lead to an alloy which shows a M_D slightly

above room temperature and a M_s far below. Now when such an alloy undergoes a plastic deformation, the formation of martensite enhances the strength of the material and prevents necking for a while.[3] If moreover one carries out a thermomechanical treatment of the austenite, in the Bay region that the T.T.T. diagram of the alloy may provide, the dislocation density is increased and a great number of sites for the nucleation of carbides are produced. When the transformation $\gamma \rightarrow \alpha'$ later on takes place, the martensite inherits most of the dislocations from the austenite, and the presence of carbides allows the spinning of some of them, while others stay relatively mobile. The result is an ultrahigh strength and a correspondingly high ductility, which are the two major striking properties of the TRIP steels: 250,000 p.s.i. at yield point and 35% elongation.[4,5]

The research program on TRIP steels has now left its primitive deductive stages for a more empirical inductive one: the properties of TRIP steels are now systematically investigated, and the results are a posteriori interpreted in the light of the TRIP phenomenon. The investigation reported here is part of this stage in the development of the research program.

To test the possibility of using a TRIP Steel in aircraft design, data on fatigue behavior under several environmental conditions were needed. This research tries to fulfill part of this program: it studies the effect of the deformation rate and of environment on the crack sensitivity of the studied alloy, under both static and dynamic fatigue.

Fracture mechanics supplied the main concepts used in the design of

the experimental program of this thesis.[6] It is why we will now review the findings of this theory relevant to this study.

Although fracture mechanics still remains a domain reserved to specialists, as is proved by the absence of a real good textbook on the subject, we will not redefine the essential concepts which it develops. We will content ourselves in speaking of the appearance of fracture surfaces and of the results obtained in applying its methods to the study of fatigue.

A linear crack propagating along its axis exhibits a fracture surface which is either flat or tilted: one speaks of fracture in a flat or shear mode. Brittle fractures by cleavage are the first type. Fracture accompanied by plastic deformation on the other hand are more difficult to classify because the aspect of the fracture surface depends upon the state of stress at the tip of the crack. In the state of plane strain, i.e. when the plastic zone has small dimensions with respect to the thickness of the material (thick sheets), the fracture propagates according to Mode I, and shows a flat surface. In the state of plane stress, i.e. when the plastic zone is greater than the thickness of the material (thin sheets), the propagates according to a combination of Modes II and III in a shear mode. Finally a combination of the shear and flat modes is often encountered: in a slab in the state of plane strain, for example, the edges are not elastically restrained, so that there the state of stress is plane; the plane of the crack, which is normally flat, becomes tilted at 45% at the edge of the slab.[7,8,9] (Fig. 1)

The study of crack propagation under fatigue stresses has benefited from two different approaches: on the one hand empirical correlations were

established between the crack propagation velocity (measured in length unit per cycle) and the stress intensity factor; on the other hand theoretical models, based for example upon the theory of continuous dislocations distribution[10] were designed. Both approaches come together to formulate or demonstrate a law in the form:

$$\frac{da}{dn} = \lambda(\Delta K)^{\nu}$$

in the case of a classical tension sinusoidal fatigue test, where λ is a function of the temperature, the environment and the strain rate among other things, and ν is a constant exponent evaluated between 1.5 and 5, with a preference for the value 4 which comes out of the dislocation model.[12,13,14] It is postulated that the fracture concept remains valid in fatigue; after the stages of initiation and slow growth, the crack becomes unstable and propagates catastrophically when the stress intensity factor reaches the value of the fracture toughness of the material.

II. MATERIAL STUDIED

We studied a TRIP Steel produced by the Crucible Steel Company. It was available in the form of sheets 0.1 inch thick.

The chemical composition reads, in weight percentage:

C	Mn	Si	Cr	Mo	Ni
0.27	0.43	0.09	11.95	1.90	7.96

Its thermomechanical processing consisted of successively:

- hammer forging between 2150 and 1800°F of the ingot into a plate 2.75 in. thick, and a hot-rolling around 2100°F until the thickness of 0.70 in.
- solution treatment at 2100°F followed by a water quench.
- hot rolling at the carefully controlled temperature of 800°F to a thickness of 0.1 in.

These stages were intended respectively to destroy the casting structure, homogenize the composition, and strain-harden the austenite to obtain the high-strength of the final product.

The knowledge of M_S and M_D allows us to further define the material. From experience, it is known that the M_S of this particular TRIP steel lies well below the boiling temperature of liquid nitrogen. On the other hand an empirical formula derived by Gerberich et al.[12] through statistical analysis of data from numerous experiments, gives an estimate of M_D. It proceeds in two steps. First M^*_{D30}, i.e. the temperature at which 30% deformation gives rise to 50% martensite in an annealed material, is calculated from:

$$M^*_{D30} = 881 - 490\ C - 18.2\ Ni - 20\ Cr - 20\ Mo - 40\ Mn$$

The result is in degrees Kelvin.

Secondly M_{D30}, the same temperature for a material which has undergone a deformation δ at temperature θ, is derived from M^{*}_{D30} through:

$$M_{D30} = M^{*}_{D30} [1 + 0.00088 \delta \theta]$$

In the case of this particular material we find that M^{*}_{D30} is 56°C and M_{D30} is 152°C.

III. EXPERIMENTAL PROCEDURE

In these experiments we tested the effects of two parameters, the strain-rate and the environment. In a first step we isolated the action of the strain-rate by pulling apart tensile specimens in air at room temperature. Then varying the two parameters, we studied their influence on fracture toughness. The fatigue experiments came afterwards under the same conditions. Finally the fracture surfaces were observed with a scanning-electron microscope. Figures 2 and 3 give a picture of the experimental set-up used during the mechanical tests.

A. Tensile Tests

Figure 4 gives a sketch of the type of specimens used. They were tested uniaxially on a "Universal Testing System," Model 901.83, of the M.T.S. Corporation. This hydraulic machine, electronically controlled by a closed-loop device, is able to supply up to 30,000 pounds to a specimen, under a load, strain or stroke control. These experiments were performed under a "full stroke" control, which insured that throughout the tests, the piston moved at a constant rate, this rate being controlled either by a ramp generator or by a function generator on which a sawtooth function had been selected. The experiments were hence carried out at constant engineering strain-rates varying from 0.006 to 10 inches per inch per minute.

B. Fracture Tests

For the fracture tests, we used the single-edge notched (SEN) specimens represented in Fig. 5. Its rather large size stems from recommendations of the ASTM for tough materials.[16]

We conducted the experiments on the same M.T.S. machine. The

environment was varied from air to distilled water (pH varying between 4.5 and 6). The strain-rate was kept constant in each experiment and varied from 0.003 to 3 inches per minute over all of them. The limatations of these values were fixed by those of the machine itself.

To determine the fracture toughness we used the following criteria: the load at which the crack became unstable was indicated by a small discontinuity in the slope of the load-displacement curve recorded during the test; the corresponding crack length was taken as the total length of the flat part of the crack, since it was observed that at the point of instability the fracture mode went from a macroscopically flat one to a shear one.

The plane-stress fracture toughness K_{CI} was computed by the following formula (Ref. 12, p. 12):

$$K = P\sqrt{a}/BW \left[1.99-0.41\left(\frac{a}{W}\right) + 18.70\left(\frac{a}{W}\right)^2 - 38.48\left(\frac{a}{W}\right)^3 + 53.85\left(\frac{a}{W}\right)^4\right] \quad (1)$$

using a FORTRAN computer program run over a Control Data 6600.

For the crack we used a corrected value which includes the effect of the plastic flow at the tip of the crack. MacClintock has given a closed form solution for Mode III, and shown that the correct value of the stress intensity factor was correctly predicted by using an expression of the crack length equal to the sum of the actual crack length and of the radius r_y of the plastic zone $\frac{1}{2\pi}\left[\frac{K_{III}}{S_y}\right]^2$. We interpolated this result to Mode I. To compute r_y we used the value of K_I obtained without any correction on a.

To simulate the perfectly flat mathematical crack for which the Formula (1) has been established, we introduced a small fatigue crack (1 or 2 mm) at the tip of the mechanical notch of the specimen.

C. Fatigue Tests

For the fatigue tests the SEN specimens were tested on the MTS machine, using a sinusoidal function and a short stroke control. During the tests we adjusted the stroke to compensate for the damping of the applied load due to the propagation of the crack. To measure the crack velocity, we made an interpolation over small crack growth lengths: at given intervals, the specimen was removed from the testing machine; we measured the progression of the crack on the surface with a traveling optical microscope and recorded the numbers of cycles run; we took the ratio of the one to the other as the crack growth rate. The stress intensity factor was calculated on the computer by the Formula (1), along with the crack growth rate, but no plastic correction was included since the material was in a state of plane strain and the load level was relatively low.

The tests were run at two different frequencies: 5 and 0.07 cycles per second. The environment was water and air. Due to the results of the tests in water, low-frequency experiments in water were additionally performed at 0°C and 60°C: A fatigue crack was grown at the tip of each specimen before any value was recorded. A typical starting value for the stress was 11,000 psi.

D. Fractography Observations

We carried out fractographic observations on representative samples of the specimens broken in all conditions, on a scanning electron microscope JEOL JSM-U3 working at 25 kilovolts. Magnification ranged from 100X to 20,000X.

IV. RESULTS AND OBSERVATIONS

Under each heading we will give the results of the experiments and describe the corresponding fracture surfaces shown by the SEM.

A. Tensile Tests

The load-displacement curves of all the specimens at various strain rates are shown in Figs. 6 to 9, and the data are summarized in Table I. It should be pointed out that they recall the shape of mild steel curves, but differ completely from austenitic steel curves.

The following features characterize those load-displacement curves:

(a) The elastic behavior slightly deviates from linearity as the load falls off in the approach of the yield point.

(b) The curves show an upper and a lower yield point.

(c) The load then settles on a Lüder's plateau between the upper and the lower yield point.

(d) After a certain amount of Lüder's displacement, a strain-hardening takes place until a maximum load is reached, after which the load falls off slightly before the actual fracture takes place.

Observation of these curves shows how they deform as the strain-rate increases: grossly speaking, the elongation during which the strain-hardening takes place decreases, leading to a smaller tensile strength and a smaller maximum elongation. The Lüder's elongation however remains constant. The effect of the strain-rate on the tensile properties is more precisely detailed in Figs. 13 to 15. The yield strength is thus shown to increase with the strain, the upper yield strength increasing at the same rate as the lower one. The tensile strength decreases as

the strain-rate increases. The same effect is shown for the elongation but the curve seems to be composed of two distinct parts separated by a transition zone between the rates of 10^{-2} and 10^{-1} inch per minute.

The fracture surfaces (Figs. 10 (a) to (d)) show all the characteristics of a plastic fracture[17,18]: macroscopically the surface is at an angle of 45° with respect to the direction of the applied load; microscopically, dimples cover the surface.

B. Toughness Tests

The load displacement curves of the toughness tests are given in Figs. 11 and 12. They show first a quasi-linear slope which decreases steadily as the load increases. The load then reaches a maximum before it decreases more and more steeply.

For the tests run in air, the specimens pulled at strain-rates under 3 inches per minute did not show any instability: the slow crack growth which accompanies the first stages of the experiment continued steadily until break of the specimen. The same phenomenon took place when we tested the specimens in water but the critical strain-rate under which no instability occurs was under 0.03 in./min. One test accidentally run with a sawtooth function of small amplitude superimposed over the linear slope, illustrates this behavior (Fig. 13): in this case the decreasing of the sawtooth function was able to stop the neck progression at any point of the load-displacement curve.

In all other tests an instability occurred, i.e. after a slow growth the crack propagated catastrophically to fracture. In most cases the fracture surface showed a transition from a flat to a shear mode, but in some cases the transition point was not so obvious (Figs. 14

and 15). Table II gives the results for the fracture toughness with a plastic zone correction.

The effect of increasing the strain-rate seems to be to lower the toughness. The scatter of the results due to the uncertainty on the measure of the critical crack length does not allow any further quantitative description. The same conclusion applies to a quantitative description of the action of water compared to the action of air.

Figures 16 to 18 give pictures of the fracture surfaces. They show ductile fracture with a slight delamination in the direction of the crack propagation for specimens tested in water. No difference was observed between the zone of high and low crack growth.

C. Fatigue Tests

1. Test Results

Table III gives the raw data collected from the tests. The results are plotted in logarithmic coordinates in Fig. 19, where the crack growth rate $\frac{da}{dn}$ is given as a function of the stress intensity factor.

The main conclusions which can be drawn from these results are the following:

(a) In high-frequency tests (5 Hz) a law of the form $\frac{da}{dn} = \lambda(\Delta K)^{\nu}$ was observed (Fig. 19a). A straight line with slope varying between 3 and 5 could fit into the experimental points, and it should be noted that because of the system of plotting chosen, a small variation in the scatter of the line led to a big variation in the value of the exponent ν. The best value found was 3.15.

(b) At the same frequency no significant difference was found between the behavior of specimens tested in air and in water.

(c) At low-frequencies (0.07 Hz) (Fig. 19b) the low number of results, due to the length of the experiments, did not permit such a detailed analysis. However the action of a lower strain-rate led obviously to higher crack growth rates for a given stress intensity factor.

(d) The crack growth rates for water tests lay higher than the one for air tests.

(e) The specimens tested in water exhibited a high temperature-sensitivity as far as the growth rate was concerned. Tests were hence run at three temperatures 0, 21 and 60°C, to see if the results would fit into a law of the form

$$\frac{da}{dn} = \mu\, e^{-\frac{\Delta G}{RT}}$$

which postulates an energy activated process. The value of the activation energy ΔG was obtained by studying the variation of $\frac{da}{dn}$ as a function of the temperature T at a constant stress intensity factor K taken as 120,000 p.s.i. $\times$ in.$^{1/2}$. The figure leads to an estimated energy of 10,200 calories per mole (Fig. 20).

2. Fractography

SEM photographs of the fracture surfaces in different cases are shown in Fig. 21 to 25.

It should be noted that:

(a) Fatigue striations were observed only on specimens tested in air at 5 Hz. Even there, they were difficult to locate because of the unevenness of the surface. In Fig. 22 the distance between two striations is about 0.5 micron. This is a microscopic measurement of the crack growth rate: 5×10^{-5} cm/cycle. Comparison with the microscopic value 8.7×10^{-5} cm/cycle shows a good accord. The slight discrepancy can be

accounted for by the fact that the length measured on the micrograph is the projection of the actual length.

(b) Delamination in the crack growth direction (Fig. 22) was observed in all the specimens tested in water and in those tested in air at low frequency. However the "intensity" of the delamination was less in air than in water, as it is easy to see by comparing the pictures taken at a magnification of 100 (Figs. 22a, 23a, 24a, and 25a).

(c) No evidence of cleavage or quasi-cleavage was found in specimens tested in water. However, tiny dimples characteristic of plastic deformation were discovered along a crack in a water tested sample. (Fig. 25).

V. INTERPRETATION

The results described above can be conveniently interpreted in the light of the accumulated knowledge about the TRIP phenomenon and of a hypothesis explaining the action of distilled water. We will first explain how the results relative to the strain-rate effects correctly fit into the picture of the TRIP transformation. Then we will show how the assumption of hydrogen embrittlement in the presence of water helps to explain the action of water. Finally at the end we will give a simple fracture mechanics calculation which allows us to estimate a lower limit of the fracture toughness, even when no crack instability occurs.

A. Strain-rate Effects and TRIP Phenomenon

A very thorough explanation of the shape of the tensile curves of TRIP steels is given by Hall.[19] Let us briefly summarize the interpretations found:

(a) The slight fall-off of the curve corresponds to the yield of the austenite, and can be compared to the beginning of the strain hardening of part of the curve of a regular austenitic steel.

(b) Then the deformation reaches a level sufficient to trigger the martensitic transformation and the material yields due to the strain of the transformation. A Lüder's band begins to propagate along the gauge length of the specimen, accompanied by a local necking; the load and the engineering stress as well decrease until the lower yield point is reached, and then settle on the Lüder's plateau.

(c) The stress remains constant until all the gauge length is affected by the transformation, i.e. until the Lüder's band reaches the other side of the gauge length.

(d) When the band reaches the bulky portion of the specimen, the load increases due to the increase of the cross section area. When this area becomes too large, the band stops and reverses its propagation using a mechanism energetically more favorable.

(e) The strain hardening then takes place with serrations superimposed on the curve. These serrations have been associated with the TRIP phenomenon,[20] with localized heating making the load drop[21] and with aging of the martensite.[19]

(f) When a large part of the austensite has transformed into martensite the specimen fails by necking when this new phase reaches its tensile strength.

We know that the nearer to M_D the temperature of an experiment is, the less martensite is formed. The heat exchange between the specimen and the environment is limited by its shape and is only slightly dependent on its temperature; hence, the greater the strain rate, the more heat is generated by plastic deformation and the higher the temperature of the specimen rises. Thus points of the gauge length of a tensile specimen, or regions ahead of the tip of the crack in an SEN specimen may experience temperatures approaching or exceeding M_D. Attempts that we made to pinpoint weld thermocouples on different specimens failed at high strain rate, but at a low strain rate(0.006 in./in./min) a temperature rise of as much as 20°C was recorded. This increase in temperature has the effect of favoring the austenite deformation more in relation to the TRIP transformation than at room temperature. The failure in uniaxial tension occurs at lower strains and hence at lower tensile strengths; in triaxial state of stress i.e., in toughness experiments the resistance to crack propagation decreases. This explains the dependence of the tensile strength,

toughness and elongation on the strain rate.

The behavior of the yield strength has to be explained in a slightly different way. Although the martensitic transformation takes place at the velocity of sound in the material, its nucleation is time sensitive. The high Y. S. observed at high strain rate can be explained by the fact that the austenite has time to further deform before the martensite transformation is made possible by enough nucleation. The same mechanism may explain the strain-rate effect on fatigue.

The particular shape of the elongation strain rate curve and the absence of instability in many toughness tests suggests that around the critical strain rates the temperature of the specimens reaches a definite neighborhood of M_D.[15]

Gerberich et al.[22] explained how the TRIP phenomenon could explain the macroscopically flat fracture mode observed in slow crack growth during toughness tests, in which case the plane stress state would suggest a shear mode. Martensite is observed to fracture first. The microfractures are assumed to form fissures in the direction of crack propagation at which point it is much easier for the crack to move laterally and connect up between fissures than to form a macroscopic shear fracture. Thus the crack continues to propagate in a flat mode as long as the volume fraction of strain-induced martensite remains high.

810,000 psi $\sqrt{\text{in.}}$. The actual value of the fracture toughness should be measurable with wider specimens.

VI. CONCLUSIONS

This investigation points out the following results:

(a) The tensile properties and toughness of a TRIP steel are strain-rate sensitive. The details of the effects observed can be correctly interpreted by the available knowledge on the TRIP phenomenon.

(b) Arguments have been given to support the assumption that in a humid environment a TRIP steel is hydrogen-embrittled.

(c) It has been shown that exceptionally high values of the plane stress fracture toughness (600 ksi $\sqrt{in.}$) can be obtained in a material exhibiting a strain-induced transformation.

Comparison of these results with the corresponding properties of conventional high-strength steels shows that:

(a) The high strength is always accompanied by a high elongation (at least 22%), whereas classical steels of comparable strengths are usually only guaranteed an elongation greater or equal to 3 to 6%.[26]

(b) The toughness of classical steels always lie under 200 ksi $\sqrt{in.}$, whereas the values found there always lie above 300 ksi $\sqrt{in.}$ and can be as high as 600 with a theoretical prediction of 800 ksi $\sqrt{in.}$.[26]

(c) The fatigue properties in air as well as in water show that the steel investigated here has a behavior comparable to that of a 12 Ni maraging steel, and are a little more resistant than a 9 Ni-46-0.25 C steel.[27]

ACKNOWLEDGMENTS

The author wishes to express his appreciation to Professor Victor F. Zackay, Professor Earl R. Parker and Mr. William W. Gerberich, for their advice and constant encouragement.

Further thanks are due to Mr. Doug Kreitz, Mrs. Gloria Pelatowski, Mrs. Shirley Ashley and Mrs. Linda LeBorgne for their help in preparing the illustrations and typing the manuscript, and to Mr. Don Krieger and Mr. Fred Park for helping me with the M.T.S. machine.

This work was supported by the U. S. Atomic Energy Commission through the Inorganic Materials Research Division of the Lawrence Radiation Laboratory.

APPENDIX

We study the fracture properties of a specimen in plane stress and Mode I. By definition of G and using the compliance C of the specimen one finds easily that:

$$G = \frac{P^2}{2} \frac{dC}{da}$$

We know furthermore that G and K_I are related by

$$G = \frac{K_I^2}{E}$$

But:

$$C = \frac{x}{P} \quad \text{and} \quad \frac{dC}{da} = \frac{1}{P} \frac{dx}{da} - \frac{x}{P^2} \frac{dP}{da}$$

Hence:

$$G = \frac{K_I^2}{E} = \frac{P}{2} \frac{dx}{da} - \frac{x}{2} \frac{dP}{da} \qquad (4)$$

A. Griffith crack

We assume first for simplicity that the stress intensity is given by $K = \frac{P}{S} \sqrt{\pi a}$, i.e. that the specimen is an elastic infinite continuum with an eliptic hole of length 2a in it. Then:

$$\frac{P^2}{S^2 E} \pi a = \frac{P}{2} \frac{dx}{da} - \frac{x}{2} \frac{dP}{da}$$

Choosing x instead of a as the variable yields:

$$\frac{2\pi}{S^2 E} a \frac{da}{dx} = \frac{1}{P} - \frac{x}{P^2} \frac{dP}{dx}$$

Now we approximate the experimental P(x) curve by:

$$P(x) = P_m \sin \frac{\pi x}{2x_m}$$

With: $P_m = 15000$ lbs

$S = 0.3$ in.^{2}

$x_m = 0.1$ in.

We are led to the solution:

$$\frac{\pi}{S^2 E} (a^2 - a_0^2) = \int_0^x \frac{dx}{P_m \sin(\frac{\pi x}{2x_m})} - \int_0^x \frac{\frac{x\pi}{2x_m} P_m \cos(\frac{\pi x}{2x_m})}{P_m^2 \sin^2 (\frac{\pi x}{2x_m})} dx$$

Elementary integrations yield

$$\frac{\pi}{S^2 E} (a^2 - a_0^2) = \frac{x}{P_m \sin (\frac{\pi x}{2x_m})} - \frac{2x_m}{\pi P_m}$$

The crack length as a function of the displacement x is given by

$$a = \left\{ a_0^2 + \frac{S^2 E}{\pi} \left[\frac{x}{P(n)} - \frac{2x_m}{\pi P_m} \right] \right\}^{1/2}$$

The knowledge of a(x) leads directly to the knowledge of K(x). A numerical computer calculation of K shows that K reaches a maximum which can be used as a lower bound of the fracture toughness, if the crack has not yet yielded catastrophically. This value is 129,000 psi/in.$^{1/2}$.

B. SEN Specimen

The actual case encountered in the experiments reported in this thesis can also be conveniently handled. Using for K the value given in Formula (1), one has to integrate the differential equation:

$$2K(a,P)\ \frac{da}{dx} = \frac{1}{P} - \frac{x}{P^2}\ \frac{dP}{dx}$$

which yields the solution:

$$\frac{2E}{S^2}\ \frac{1.99}{2}\ (a^2-a_0{}^2) - \frac{0.61}{3W}\ (a^3-a_0{}^3) + \frac{18.70}{4W^2}\ (a^6-a_0{}^6)$$

$$- \frac{38.68}{5W^3}\ (a^5-a_0{}^5) + \frac{53.85}{6W^4}\ (a^6-a_0{}^6) =$$

$$\frac{x}{P_m \sin(\frac{\pi x}{2x_m})} - \frac{2x_m}{\pi P_m}$$

A numerical computer calculation shows that K increases steadily, until x reaches a value greater than 0.7 W, in which case Formula (1) is no longer valid. What happens physically is that the plastic zone then covers the whole cross section of the specimen which then fails by deformation of the entire section; it is no longer possible to measure a fracture toughness value. However, the value of K for a crack length of 0.7 W is a lower bound for the fracture toughness. The value found without any plastic correction was 370,000 psi in.$^{1/2}$, and with the plastic correction it was 810,000 psi/in.$^{1/2}$.

REFERENCES

1. T. Angel, Formation of Martensite in Austenitic Stainless Steels, J. Iron & Steel Inst. 177, 165 (1954).

2. V. F. Zackay, W. W. Gerberich, R. Busch and E. R. Parker, The Strength and Toughness of Dynamically Strain-aged Alloy Steels, Proc. 1st Intl. Conf. on Fracture, Sendai (Japan), 2, 813 (1965).

3. J. A. Hall, V. F. Zackay and E. R. Parker, Structural Observations in a Metastable Steel, ASM Trans. Quat. 4, 62, 965 (1969).

4. V. F. Zackay, E. R. Parker, D. Fahr and R. Busch, The Enhancement of Ductility in High Strength Steels, ASM Trans. Quat. 2, 60 (1967).

5. W. W. Gerberich, P. L. Hemmings, M. D. Merz, and V. F. Zackay, Preliminary Toughness Results on TRIP Steel, Trans. ASM 61 , 843 (1968).

6. I. Finnie, Use of Elastic Solutions for Fracture Prediction, Notes for the UC Extension Course on Fracture, April 1969.

7. J. Malkin, G. Sanz, Introduction ă la mécanique des ruptures, Rev. Metal. 67è année, 4, 313 (1970).

8. F. Erdogan and G. C. Sih, On the Crack Extension in Plates Under Plane Loading and Transverse Shear, Trans. ASME, J. Basic Engr., 85, 519 (1963).

9. J. I. Bluhm, A Model for the Effect of Thickness on Fracture Toughness, Proc ASM 61, 1324 (1961).

10. J. Weertman, Rate of Growth of Fatigue Cracks Calculated from the Theory of Infinitesimal Dislocations Distributed on a Plane, Proc. 1st Intl. Conf. on Fracture, Sendai (Japan) 1, 153 (1965).

11. B. A. Bilby, et al., The Spread of Plastic Yield from a Notch, Proc. Roy. Soc. (London) A 272, 304 (1963).

12. J. R. Rice, Mechanics of Crack Tip Deformation and Extension by Fatigue, in ASTM STP415, p. 247, 1966.

13. P. Paris and F. Erdogan, A Critical Analysis of Crack Propagation Laws, Trans. ASME, J. Basic Engr. 85, 528 (1963).

14. A. S. Tetelman and A. J. McEvily, Fracture of Structural Materials, (Wiley and Sons, 1967) Chap. 8, p. 347.

15. W. W. Gerberich, G. Thomas, E. R. Parker and V. F. Zackay, Metastable Austenites : Decomposition and Strength, to be published in the Proc. of the 2nd Intl. Conf. on the Strength of Metals and Alloys, Pacific Grove, Calif., Sept. 1970 and UCRL-20308.

16. W. F. Brown and J. E. Stanley, Plane Strain Crack Toughness Testing of High Strength Metallic Materials, ASTM STP No. 410, 1966.

17. R. M. N. Pelloux, The Analysis of Fracture Surfaces by Electron Microscopy, Boeing Research Scientific Laboratories, D1-82-0169-R1, Dec. 1963.

18. C. D. Beachem and R. M. N. Pelloux, Electron Fractography, in ASTM STP381, p. 210, June 1964.

19. G. R. Chanani, M. S. Thesis, University of California, Berkeley, UCRL-17805, Sept. 1967.

20. J. Bressanelli and A. Moskowitz, Effects of Strain Rate, Temperature and Composition on Tensile Properties of Metastable Austenitic Steels, Trans. ASM 59, 223 (1966).

21. W. W. Gerberich, P. L. Hemmings, V. F. Zackay and E. R. Parker, Interactions Between Crack Growth and Strain-Induced Transformation, UCRL-18467, Sept. 1968.

22. P. Bastien, La Rupture Différée des Aciers en présence d'hydrogène et son mécanisme, in "L'Hydrogène dans les Métaux," Valduc, France, Sept. 1967, published by "Centre d'Etudes de Bruyères-le-Châtel".

23. R. A. McCoy, W. W. Gerberich and V. F. Zackay, On the Resistance of TRIP Steel to Hydrogen Embrittlement, Met. Trans 1, 7, 2031 (1970).

24. R. A. McCoy, personal communication (August 1970).

25. R. A. Oriani, Hydrogen in Metals, in Proc. Conference on Fundamental Aspects of Stress Corrosion Cracking, Ohio State University, Sept. 1967, p. 32.

26. Aerospace Structural Metals Handbook, Syracuse University Press, Ferrous Alloy PH 15-7 Mo, Code 1503 (1966).

27. T. W. Crooker and E. A. Lange, The Influence of Salt Water in Fatigue Crack Growth in High-Strength Steels, in ASTM STP662, p. 258 (1970).

Table I. Tensile properties

Strain rate (in./in./min)	Upper Yield (psi)	Lower Strength (psi)	Tensile Strength (psi)	Elongation (%)
0.003	208,800	201,100	235,500	47.8
0.01	211,800	202,000	235,800	46.6
0.04	209,800	193,100	226,600	35.0
0.1	209,800	199,300	212,700	27.8
0.25	216,400	204,800	218,100	26.7
1.0	212,800	202,700	221,800	30.8
1.0	212,800	204,500	206,100	22.2
10	221,000	206,500	217,600	23.9

Table II. Fracture toughness data.

Water				Air		
Crosshead rate (in./min)	Critical crack length (in.)	Critical load (lbs.)	Fracture toughness (psi $in.^{1/2}$)	Critical crack length (in.)	Critical load (lbs)	Fracture toughness (psi $in.^{1/2}$)
0.003	no instability			no instability		
0.03	1.69	17,500	610,500	no instability		
0.03	1.55	17,500	476,300	no instability		
0.3	1.36	15,500	312,100	no instability		
3	1.55	16,600	449,500	1.55	18,000	498,400

Table III. Results of the fatigue tests

a. The maximum load is the load at infinity at the beginning of the test.

b. The loading stress is the corresponding stress.

c. CRACK INCRE stands for Crack increment. It is expressed in centimeters.

d. The stress intensity factor is expressed in kgf $mm^{-3/}$ and psi $in.^{1/2}$.

e. The first line of results gives the values of the relevant quantities before the tests start.

f. E+(n) stands for 10^{+n}.

Table III.

SPECIMEN NUMBER	2	
TESTED IN OPEN AIR		
FREQUENCY	5.000	HERTZ
MAXIMUM LOAD	3540	POUNDS
LOADING STRESS	11931.244	P.S.I.
THICKNESS	.0989	INCH
ORIGINAL CRACK LENGTH	2.54000	CM

N	CRACK INCRE	CRACK LENGTH CM	CRACK LENGTH IN	CYCLES HERTZ	CRACK GROWTH RATE PER CYCLE CM/CYCLE	CRACK GROWTH RATE PER CYCLE IN/CYCLE	STRESS INTENSITY FACTOR KGF(MM)-3/2	STRESS INTENSITY FACTOR PSI(IN)+1/2
0	0.	2.5400	1.0000	0	0.	0.	1.3469E+02	3.7928E+04
1	.2280	2.7680	1.0898	6096	3.7402E-05	1.4725E-05	1.2893E+02	3.6307E+04
2	.1952	2.9632	1.1666	4678	4.1727E-05	1.6428E-05	1.4730E+02	4.1478E+04
3	.2660	3.2292	1.2713	3251	8.1821E-05	3.2213E-05	1.6304E+02	4.5912E+04
4	.2810	3.5102	1.3820	3002	9.3604E-05	3.6852E-05	1.9016E+02	5.3547E+04
5	.3540	3.8642	1.5213	3069	1.1535E-04	4.5412E-05	2.2520E+02	6.3415E+04
6	.3220	4.1862	1.6481	1563	2.0601E-04	8.1108E-05	2.7986E+02	7.8806E+04
7	.5000	4.6862	1.8450	1036	4.8263E-04	1.9001E-04	3.5248E+02	9.9256E+04
8	.3640	5.0502	1.9883	1264	2.8797E-04	1.1338E-04	4.7733E+02	1.3441E+05

XBL 709-6535

Table III (continued)

SPECIMEN NUMBER	10	
TESTED IN OPEN AIR		
FREQUENCY	5.000	HERTZ
MAXIMUM LOAD	7080	POUNDS
LOADING STRESS	23862.487	P.S.I.
THICKNESS	.0989	INCH
ORIGINAL CRACK LENGTH	2.54000	CM

N	CRACK INCRE	CRACK LENGTH CM	CRACK LENGTH IN	CYCLES HERTZ	CRACK GROWTH RATE PER CYCLE CM/CYCLE	CRACK GROWTH RATE PER CYCLE IN/CYCLE	STRESS INTENSITY FACTOR KGF(MM)-3/2	STRESS INTENSITY FACTOR PSI(IN)+1/2
0	0.	2.5400	1.0000	0	0.	0.	2.7145E+02	7.6439E+04
1	*.0644	2.7036	1.0644	703	2.3268E-04	9.1607E-05	2.8697E+02	8.0810E+04

SPECIMEN NUMBER	1T	
TESTED IN OPEN AIR		
FREQUENCY	5.000	HERTZ
MAXIMUM LOAD	4720	POUNDS
LOADING STRESS	15908.325	P.S.I.
THICKNESS	.0989	INCH
ORIGINAL CRACK LENGTH	2.70358	CM

N	CRACK INCRE	CRACK LENGTH CM	CRACK LENGTH IN	CYCLES HERTZ	CRACK GROWTH RATE PER CYCLE CM/CYCLE	CRACK GROWTH RATE PER CYCLE IN/CYCLE	STRESS INTENSITY FACTOR KGF(MM)-3/2	STRESS INTENSITY FACTOR PSI(IN)+1/2
0	0.	2.7036	1.0644	0	0.	0.	1.9526E+02	5.4984E+04
1	*.0757	2.8958	1.1401	5247	3.6636E-05	1.4423E-05	2.1032E+02	5.9226E+04
2	*.1862	3.3689	1.3263	2135	2.2157E-04	8.7232E-05	2.6323E+02	7.4125E+04
3	*.1221	3.6791	1.4484	1029	3.0144E-04	1.1868E-04	3.1585E+02	8.8940E+04
4	*.2514	4.3175	1.6998	1001	6.3782E-04	2.5111E-04	4.4736E+02	1.2597E+05

XBL 709-6539

Table III (continued)

SPECIMEN NUMBER	10	
TESTED IN OPEN AIR		
FREQUENCY	.070	HERTZ
MAXIMUM LOAD	7000	POUNDS
LOADING STRESS	25925.926	P.S.I.
THICKNESS	.0900	INCH
ORIGINAL CRACK LENGTH	3.31000	CM

N	CRACK INCRE	CRACK LENGTH CM	CRACK LENGTH IN	CYCLES HERTZ	CRACK GROWTH RATE PER CYCLE CM/CYCLE	CRACK GROWTH RATE PER CYCLE IN/CYCLE	STRESS INTENSITY FACTOR KGF(MM)-3/2	STRESS INTENSITY FACTOR PSI(IN)+1/2
0	0.	3.3100	1.3031	0	0.	0.	4.4002E+02	1.2391E+05
1	.5300	3.8400	1.5118	1000	5.3000E-04	2.0866E-04	3.9778E+02	1.1201E+05

SPECIMEN NUMBER	10	
TESTED IN OPEN AIR		
FREQUENCY	.070	HERTZ
MAXIMUM LOAD	9950	POUNDS
LOADING STRESS	36851.852	P.S.I.
THICKNESS	.0900	INCH
ORIGINAL CRACK LENGTH	3.84000	CM

N	CRACK INCRE	CRACK LENGTH CM	CRACK LENGTH IN	CYCLES HERTZ	CRACK GROWTH RATE PER CYCLE CM/CYCLE	CRACK GROWTH RATE PER CYCLE IN/CYCLE	STRESS INTENSITY FACTOR KGF(MM)-3/2	STRESS INTENSITY FACTOR PSI(IN)+1/2
0	0.	3.8400	1.5118	0	0.	0.	8.6771E+02	2.4434E+05
1	.9950	4.8350	1.9035	60	1.6583E-02	6.5288E-03	8.1102E+02	2.2838E+05

XBL 709-6536

Table III (continued)

SPECIMEN NUMBER	53	
TESTED IN DISTILLED WATER		
FREQUENCY	.070	HERTZ
MAXIMUM LOAD	7000	POUNDS
LOADING STRESS	26070.764	P.S.I.
THICKNESS	.0895	INCH
ORIGINAL CRACK LENGTH	2.74700	CM

N	CRACK INCRE	CRACK LENGTH CM	CRACK LENGTH IN	CYCLES HERTZ	CRACK GROWTH RATE PER CYCLE CM/CYCLE	CRACK GROWTH RATE PER CYCLE IN/CYCLE	STRESS INTENSITY FACTOR KGF(MM)-3/2	STRESS INTENSITY FACTOR PSI(IN)+1/2
0	0.	2.7470	1.0815	0	0.	0.	3.2987E+02	9.2890E+04
1	.0330	2.7800	1.0945	100	3.3000E-04	1.2992E-04	3.2436E+02	9.1338E+04

SPECIMEN NUMBER	51	
TESTED IN DISTILLED WATRE		
FREQUENCY	.070	HERTZ
MAXIMUM LOAD	7000	POUNDS
LOADING STRESS	24054.983	P.S.I.
THICKNESS	.0970	INCH
ORIGINAL CRACK LENGTH	2.54920	CM

N	CRACK INCRE	CRACK LENGTH CM	CRACK LENGTH IN	CYCLES HERTZ	CRACK GROWTH RATE PER CYCLE CM/CYCLE	CRACK GROWTH RATE PER CYCLE IN/CYCLE	STRESS INTENSITY FACTOR KGF(MM)-3/2	STRESS INTENSITY FACTOR PSI(IN)+1/2
0	0.	2.5492	1.0036	0	0.	0.	2.7495E+02	7.7425E+04
1	.9140	3.4632	1.3635	415	2.2024E-03	8.6709E-04	1.6017E+02	4.5104E+04
2	.4050	3.8682	1.5229	122	3.3197E-03	1.3070E-03	4.2860E+02	1.2069E+05

SPECIMEN NUMBER	50	
TESTED IN DISTILLED WATER		
FREQUENCY	.070	HERTZ
MAXIMUM LOAD	7000	POUNDS
LOADING STRESS	25641.026	P.S.I.
THICKNESS	.0910	INCH
ORIGINAL CRACK LENGTH	2.70000	CM

N	CRACK INCRE	CRACK LENGTH CM	CRACK LENGTH IN	CYCLES HERTZ	CRACK GROWTH RATE PER CYCLE CM/CYCLE	CRACK GROWTH RATE PER CYCLE IN/CYCLE	STRESS INTENSITY FACTOR KGF(MM)-3/2	STRESS INTENSITY FACTOR PSI(IN)+1/2
0	0.	2.7000	1.0630	0	0.	0.	3.1666E+02	8.9170E+04
1	.6480	3.3480	1.3181	58	1.1172E-02	4.3986E-03	2.5910E+02	7.2962E+04
2	.5410	3.8890	1.5311	50	1.0820E-02	4.2598E-03	4.2174E+02	1.1876E+05

XBL 709-6537

Table III (continued)

SPECIMEN NUMBER	11	
TESTED IN DISTILLED WATER		
FREQUENCY	5.000	HERTZ
MAXIMUM LOAD	4000	POUNDS
LOADING STRESS	14652.015	P.S.I.
THICKNESS	.0910	INCH
ORIGINAL CRACK LENGTH	2.54000	CM

N	CRACK INCRE	CRACK LENGTH CM	CRACK LENGTH IN	CYCLES HERTZ	CRACK GROWTH RATE PER CYCLE CM/CYCLE	CRACK GROWTH RATE PER CYCLE IN/CYCLE	STRESS INTENSITY FACTOR KGF(MM)-3/2	STRESS INTENSITY FACTOR PSI(IN)+1/2
0	0.	2.5400	1.0000	0	0.	0.	1.6562E+02	4.6638E+04
1	.0380	2.5780	1.0150	1076	3.5316E-05	1.3904E-05	1.6407E+02	4.6201E+04

SPECIMEN NUMBER	30	
TESTED IN DISTILLED WATER		
FREQUENCY	5.000	HERTZ
MAXIMUM LOAD	3540	POUNDS
LOADING STRESS	13409.091	P.S.I.
THICKNESS	.0880	INCH
ORIGINAL CRACK LENGTH	2.54000	CM

N	CRACK INCRE	CRACK LENGTH CM	CRACK LENGTH IN	CYCLES HERTZ	CRACK GROWTH RATE PER CYCLE CM/CYCLE	CRACK GROWTH RATE PER CYCLE IN/CYCLE	STRESS INTENSITY FACTOR KGF(MM)-3/2	STRESS INTENSITY FACTOR PSI(IN)+1/2
0	0.	2.5400	1.0000	0	0.	0.	1.5148E+02	4.2655E+04
1	.5770	3.1170	1.2272	6625	8.7094E-05	3.4289E-05	1.2807E+02	3.6064E+04
2	.3070	3.4240	1.3480	2238	1.3718E-04	5.4006E-05	1.9976E+02	5.6251E+04
3	.4840	3.9080	1.5386	1517	3.1905E-04	1.2561E-04	2.3952E+02	6.7447E+04
4	.4050	4.3130	1.6980	1009	4.0139E-04	1.5803E-04	3.2629E+02	9.1880E+04

SPECIMEN NUMBER	9	
TESTED IN DISTILLED WATER		
FREQUENCY	5.000	HERTZ
MAXIMUM LOAD	4000	POUNDS
LOADING STRESS	14492.754	P.S.I.
THICKNESS	.0920	INCH
ORIGINAL CRACK LENGTH	2.54000	CM

N	CRACK INCRE	CRACK LENGTH CM	CRACK LENGTH IN	CYCLES HERTZ	CRACK GROWTH RATE PER CYCLE CM/CYCLE	CRACK GROWTH RATE PER CYCLE IN/CYCLE	STRESS INTENSITY FACTOR KGF(MM)-3/2	STRESS INTENSITY FACTOR PSI(IN)+1/2
0	0.	2.5400	1.0000	0	0.	0.	1.6381E+02	4.6128E+04
1	.0610	2.6010	1.0240	1078	5.6586E-05	2.2278E-05	1.6171E+02	4.5536E+04

XBL 709-6538

FIGURE CAPTIONS

Fig. 1. Typical aspects of fracture surfaces. The fracture is initiated at a fatigue notch following a mechanical notch.

(a) Flat fracture mode.

(b) Shear fracture mode.

(c) Transition from a flat to a shear mode.

(d) The sides of the specimen break in a shear mode, whereas the middle breaks in a flat mode.

Fig. 2. Experimental setting for a toughness test in water on the Universal Testing Machine.

Fig. 3. Control Panel of the Universal Testing Machine.

Fig. 4. Tensile specimen. The thickness varied around 0.095 in.

Fig. 5. Fracture toughness specimen. The thickness varied around 0.095 in.

Fig. 6. Load displacement curves of tensile specimens at various strain rates.

(a) 10 in./in./min

(b) 1 in./in./min

(c) 0.25 in./in./min

(d) 0.1 in./in./min

(e) 0.04 in./in./min

(f) 0.01 in./in./min

(g) 0.006 in./in./min

Fig. 7. Lower and upper yield strengths as a function of the strain rate.

Fig. 8. Tensile strength as a function of the strain rate.

Fig. 9. Elongation as a function of the strain rate.

Fig. 10. Aspect of the fracture surface of a tensile specimen and SEM micrographs of the fracture surface of a tensile specimen.

Fig. 11. Load-displacement curves of SEN specimens tested in air at various crosshead rates:

(a) 3 in./min

(b) 0.3 in./min

(c) 0.03 in./min

(d) 0.003 in./min

Fig. 12. Load-displacement curves of SEN specimens tested in water at various crosshead rates:

(a) 3 in./min

(b) 0.3 in./min

(c) 0.03 in./min

(d) 0.003 in./min

Fig. 13. Load displacement curve of a SEN specimen tested in air. During the test the crosshead rate increased according to a law composed of a linear part and a superimposed sawtooth function of small amplitude.

Fig. 14. Aspect of the fracture surfaces of SEN specimens showing an instability in a fracture test. Both sides of the surface are shown. From left to right the specimens have the following history:

- 3×10^{-2} in./min - air
- 3×10^{-1} in./min - air
- 3×10^{-2} in./min - air
- 3 in./min - air
- 3 in./min - water

Fig. 15. The same surfaces at a higher magnification.

(a) Tested at 3 in./min in air.

(b) Tested at 3 in./min in water.

(c) Tested at 0.3 in./min in air.

In (a), (b) and (c) a transition from a flat to a shear mode is visible.

(d) 0.003 in./min in air.

The transition between flat and shear modes is not too obvious.

Fig. 16. SEM micrographs of the fracture surface of a SEN specimen tested in air at 3 in./min for toughness measurements. The pictures are taken from the slow growth zone.

Fig. 17. SEM micrographs of the fracture surface of a SEN specimen tested in air at 3 in./min for toughness measurement. The pictures are taken from the fast growth zone.

Fig. 18. SEM micrographs of the fracture surface of a SEN specimen tested in water at 3 in./min for toughness measurements. The pictures are taken from the slow growth zone.

Fig. 19. Fatigue results plotted in log-log coordinated as crack growth rate versus the stress intensity factor.

(a) Results obtained at 5 cycles/sec.

(b) Results obtained at 0.07 cycles/sec at different temperatures.

Fig. 20. Crack growth rate versus inverse of absolute temperature. The slope of the straight line is the activation energy of the process divided by the gas constant.

Fig. 21. SEM micrograph of the fracture surface of a SEN specimen fatigued in air at 5 cycles/sec.

Fig. 22. SEM micrographs of the fracture surface of a SEN specimen fatigued in water at 5 cycles/sec.

Fig. 23. SEM micrographs of the fracture surface of a SEN specimen fatigued in distilled water at 5 cycles/sec.

Fig. 24. SEM micrographs of the fracture surface of a SEN specimen fatigued in water at 21°C and 0.07 cycles/sec.

Fig. 25. SEM micrographs of the fracture surface of a SEN specimen fatigued in air at 21°C and 0.07 cycles/sec.

Fig. 26. Fracture surface aspect of a comparable steel which failed in tension in an hydrogen atmosphere. (This picture courtesy of McCoy.)

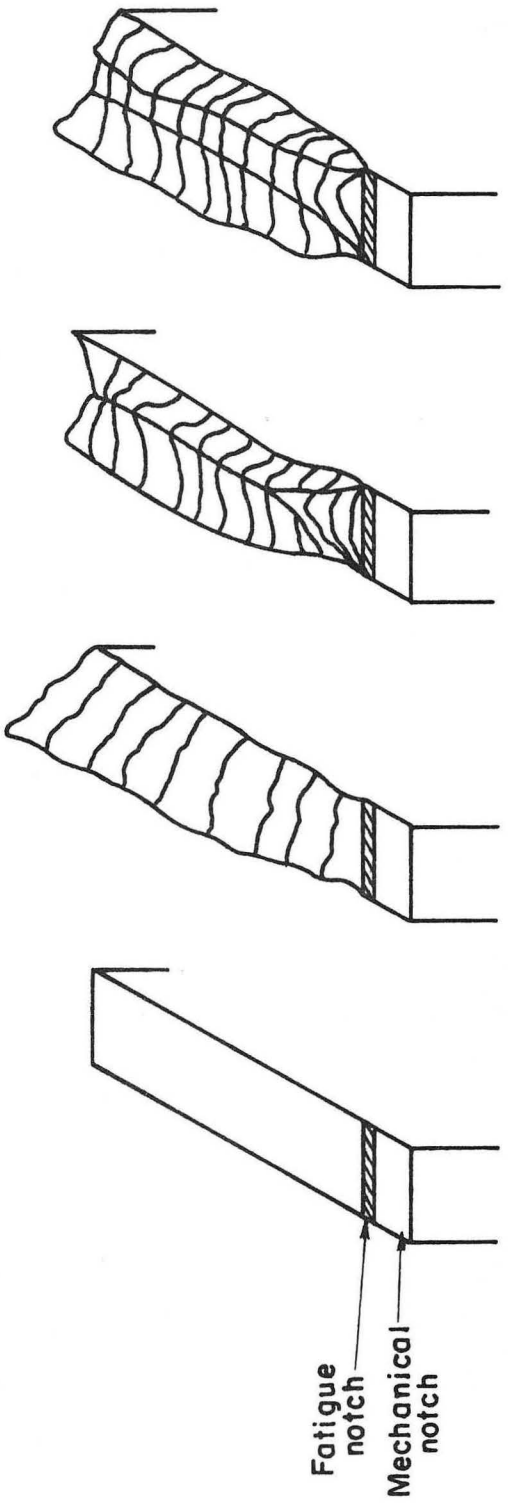

XBL 709-6522

Fig. 1

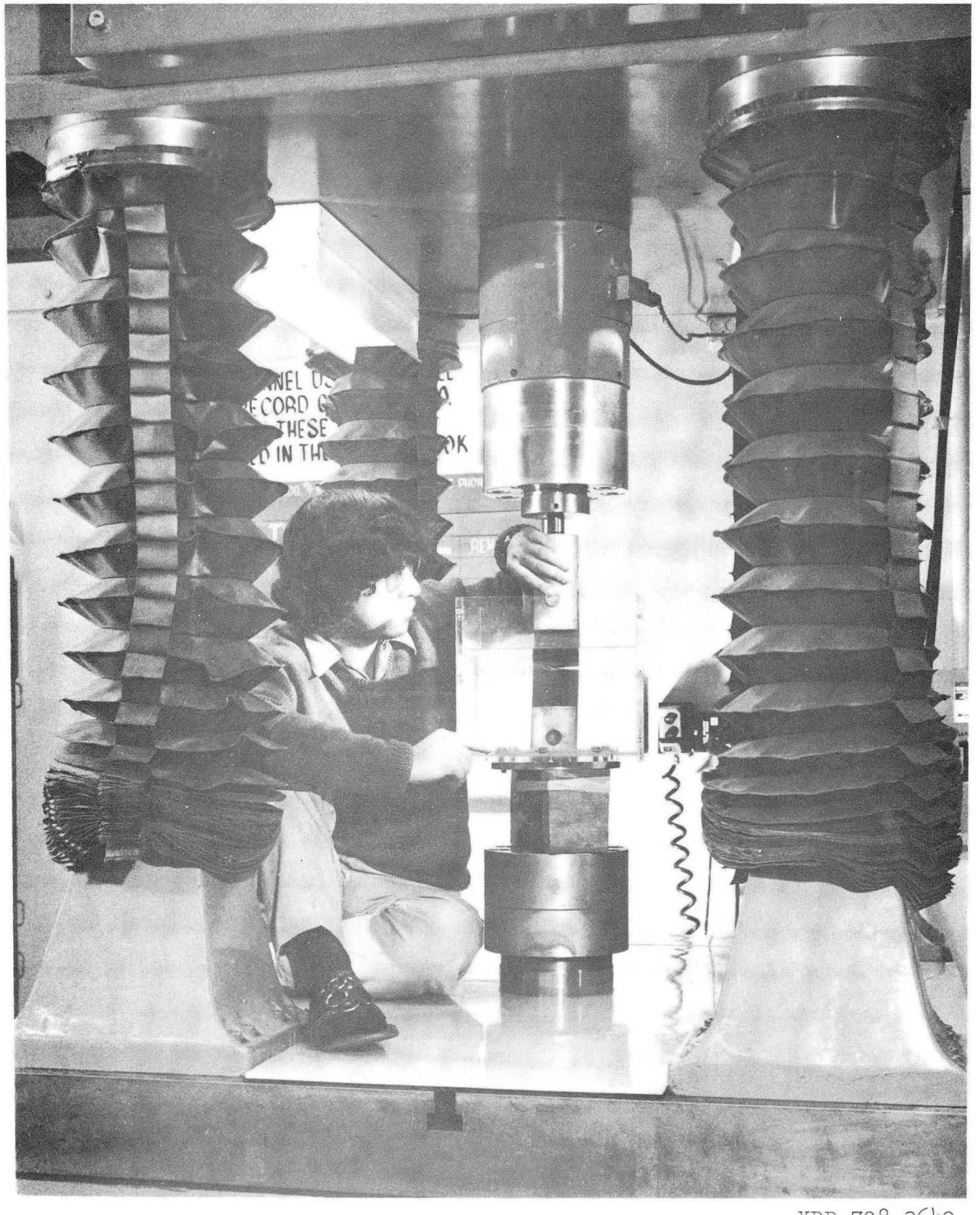

XBB 708-3649

Fig. 2

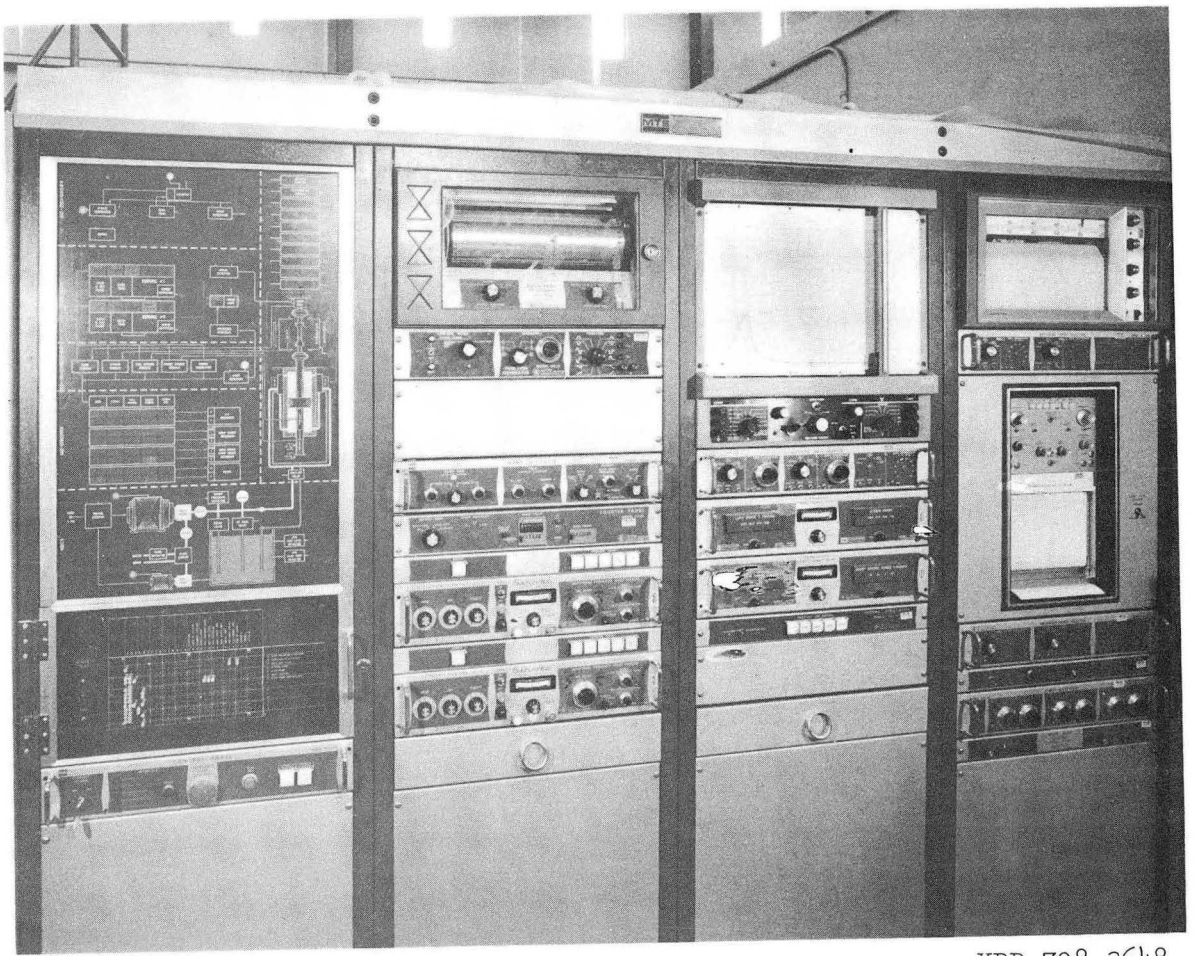

XBB 708-3648

Fig. 3

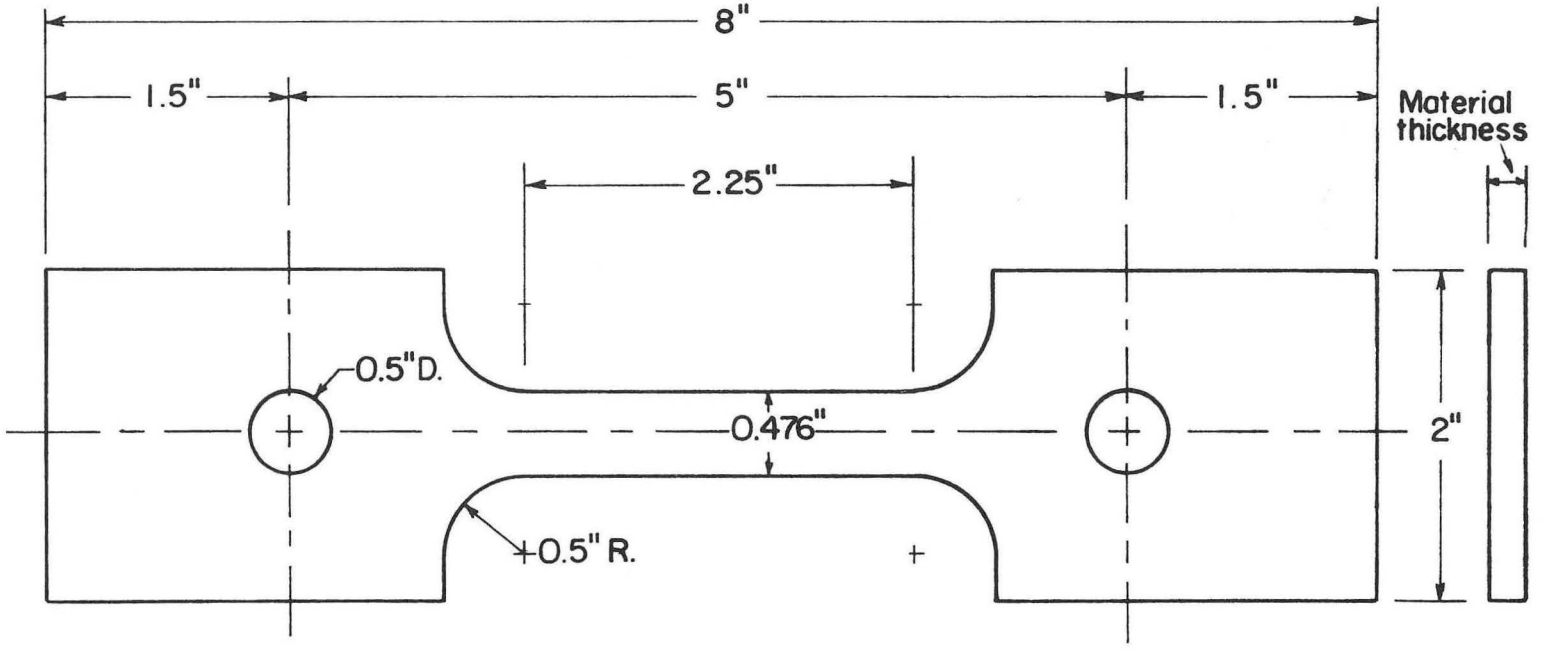

XBL 709-6524

Fig. 4

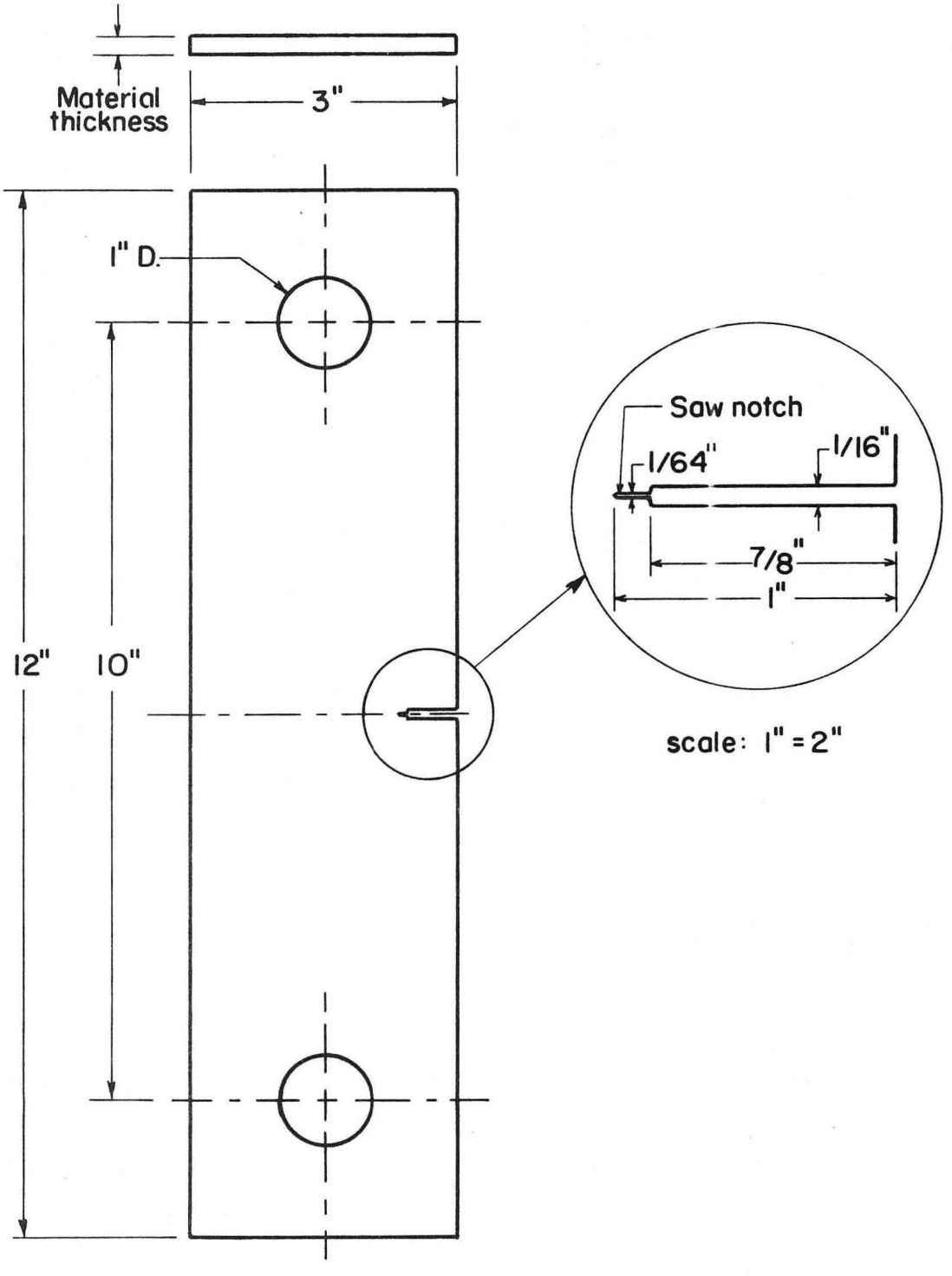

XBL 709-6523

Fig. 5

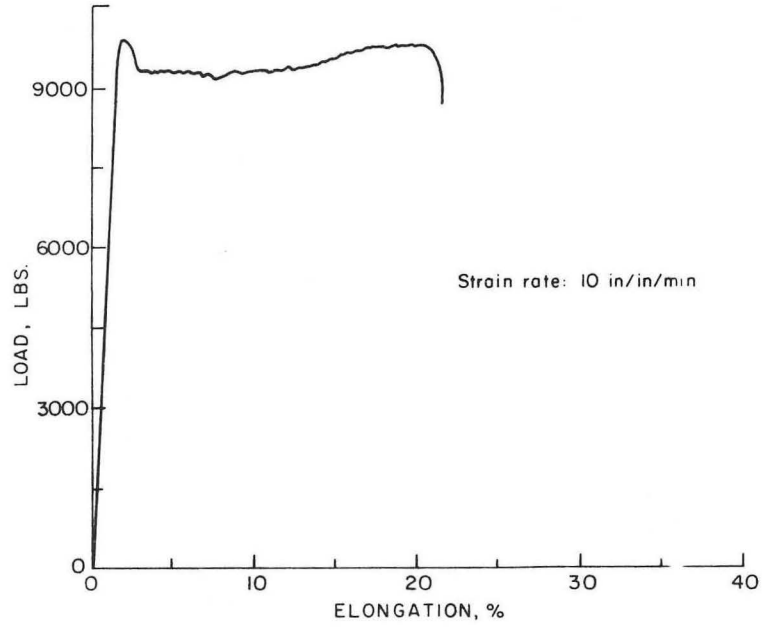

(a)

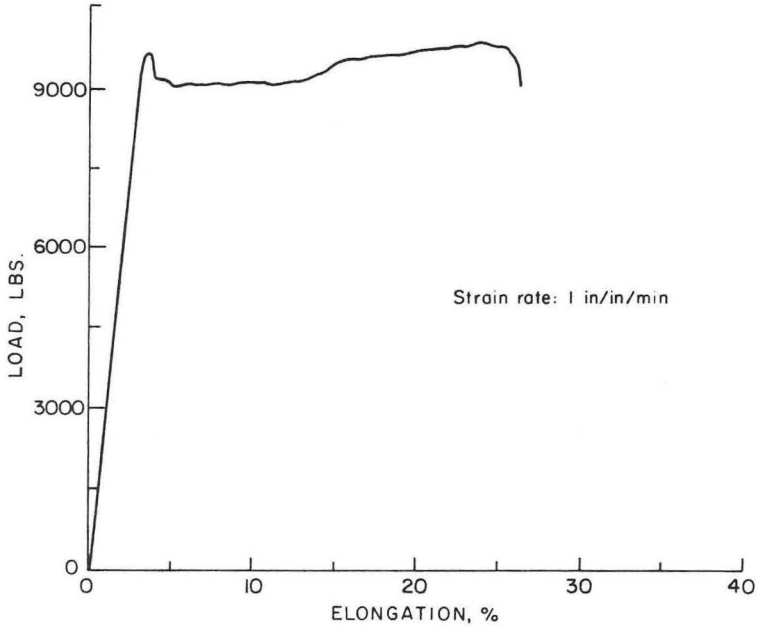

XBL 709-6534

(b)

Fig. 6

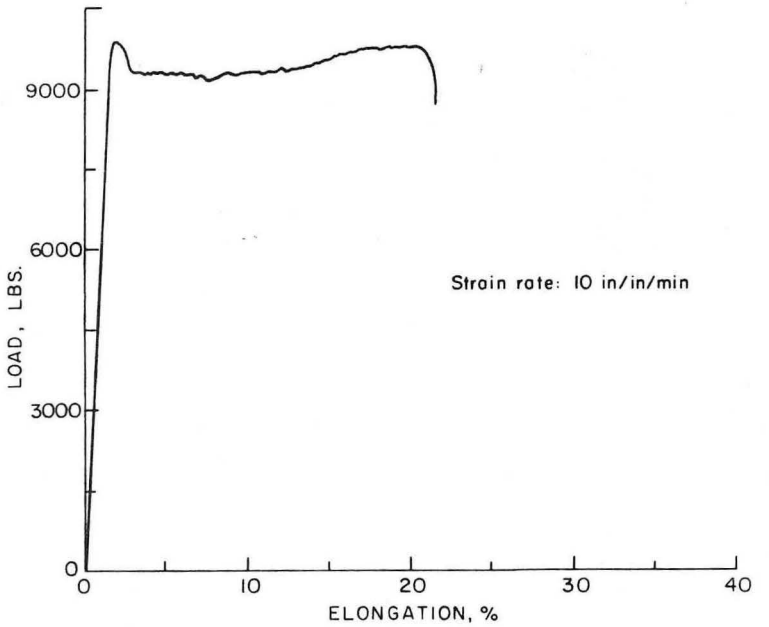

(c)

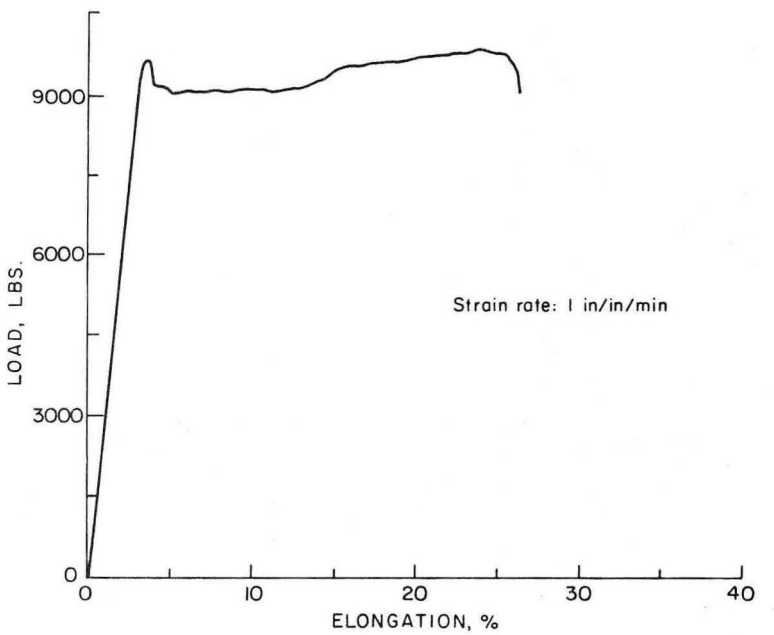

XBL 709-6534

(d)

Fig. 6 (continued)

(e)

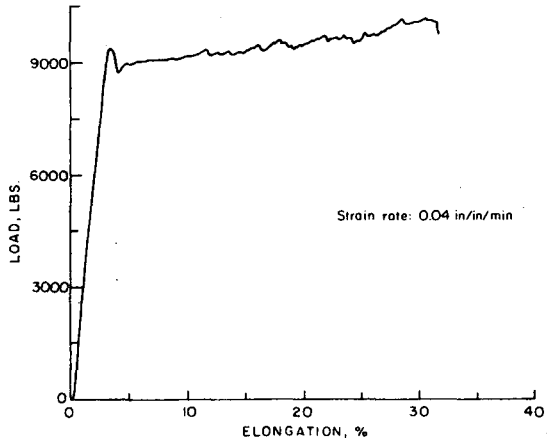

(f)

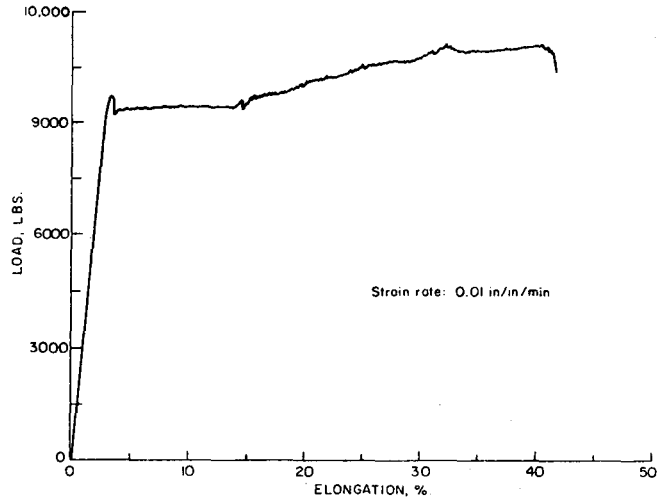

(g)

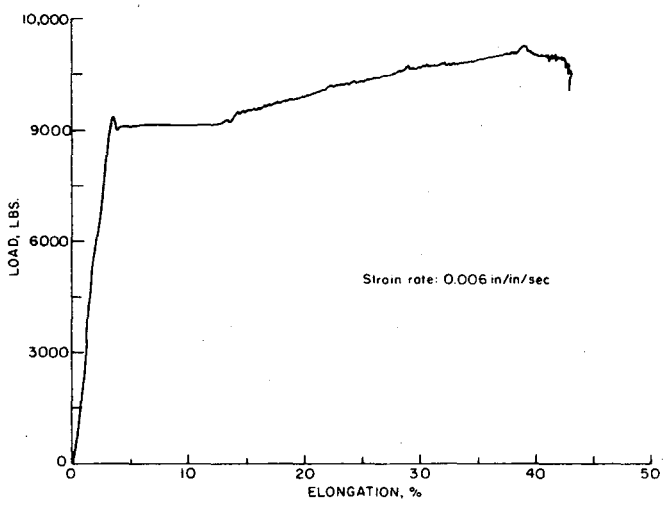

XBL 709-6532

Fig. 6 (continued)

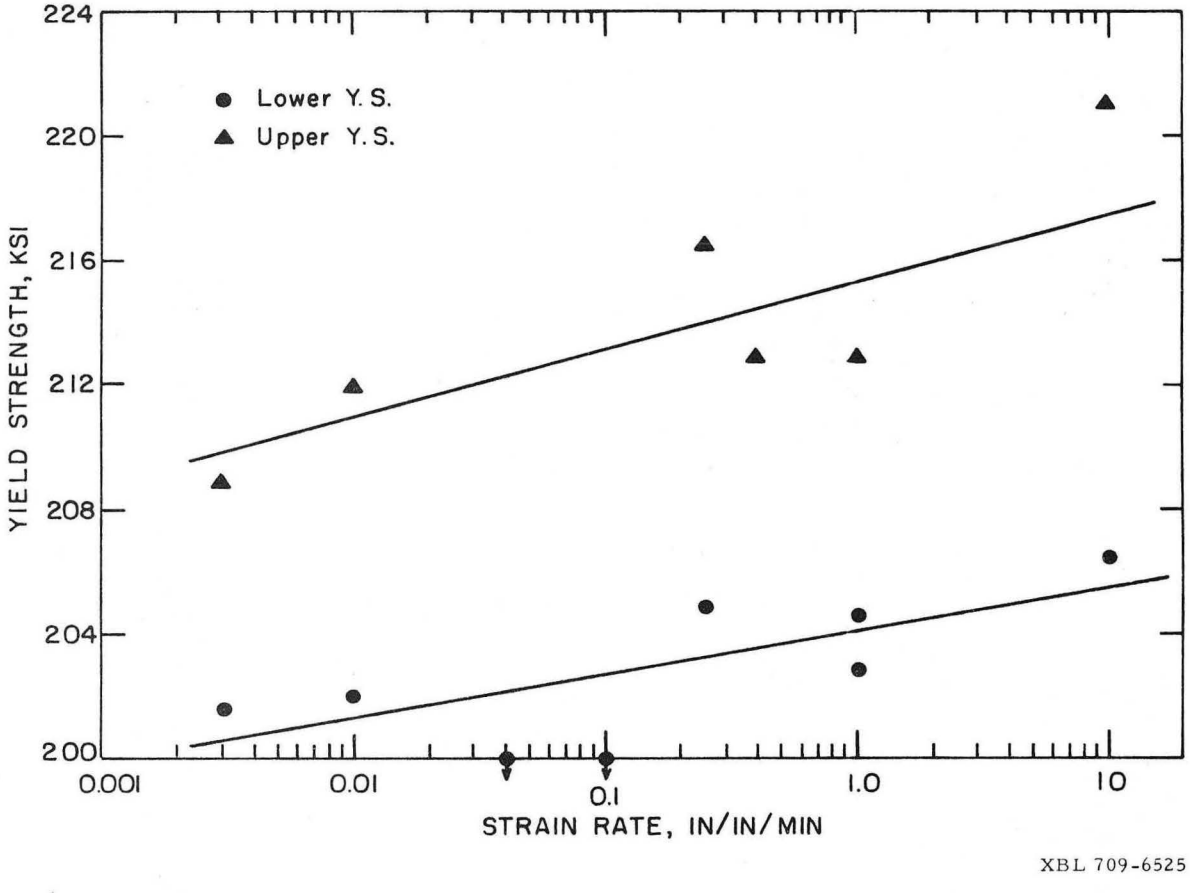
224
220
216
212
208
204
200
YIELD STRENGTH, KSI
Lower Y.S.
Upper Y.S.
0.001
0.01
0.1
1.0
10
STRAIN RATE, IN/IN/MIN
XBL 709-6525

Fig. 7

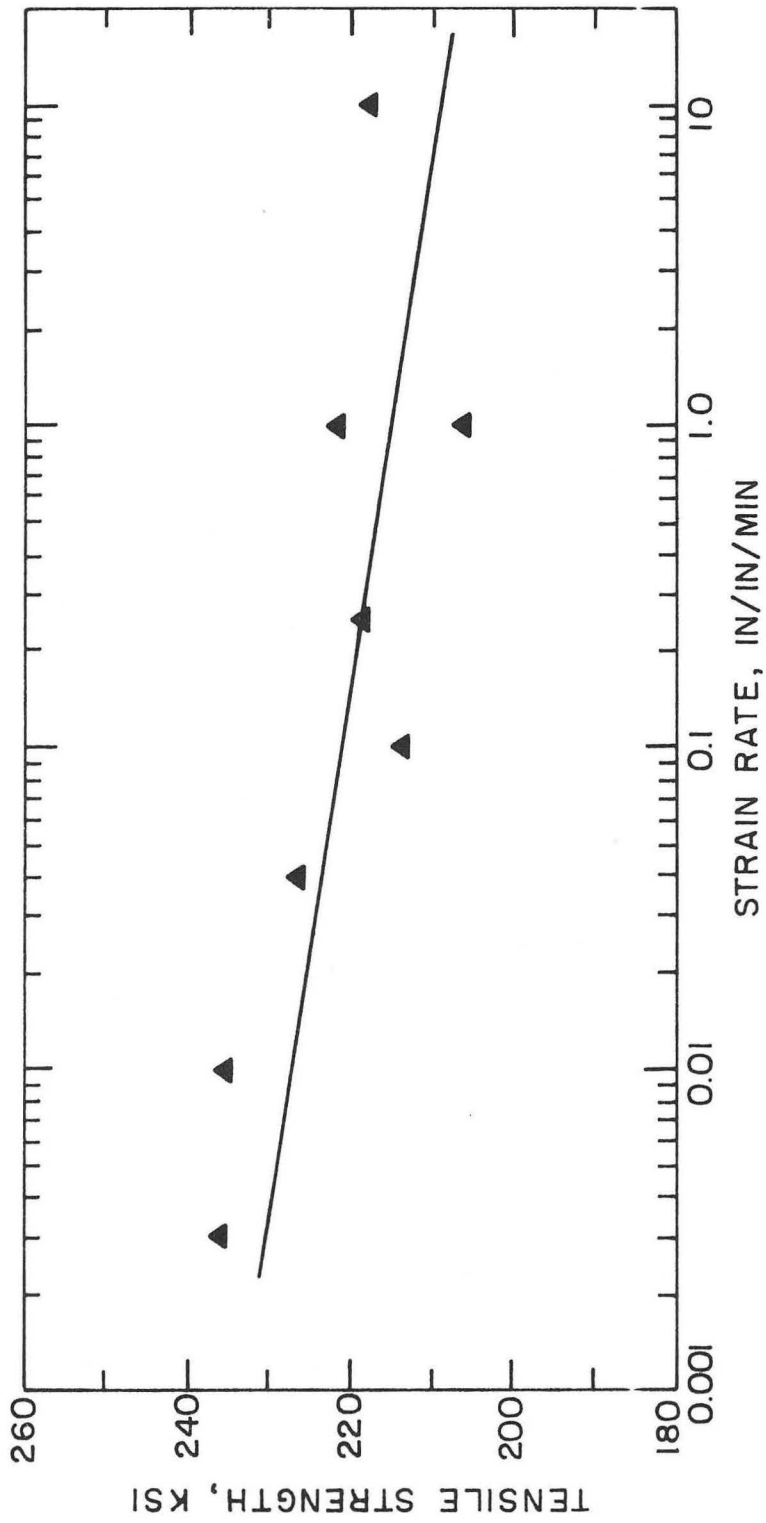

XBL 709-6526

Fig. 8

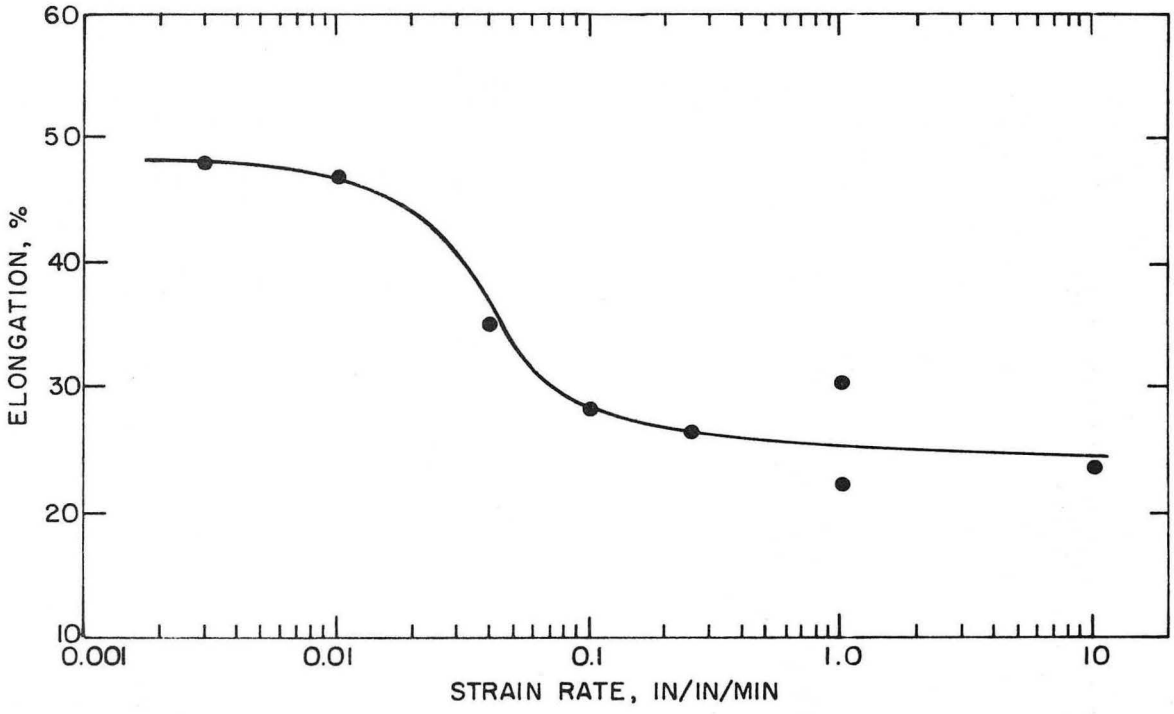
60
50
40
30
20
10
ELONGATION, %
0.001
0.01
0.1
1.0
10
STRAIN RATE, IN/IN/MIN
XBL 709-6527

Fig. 9

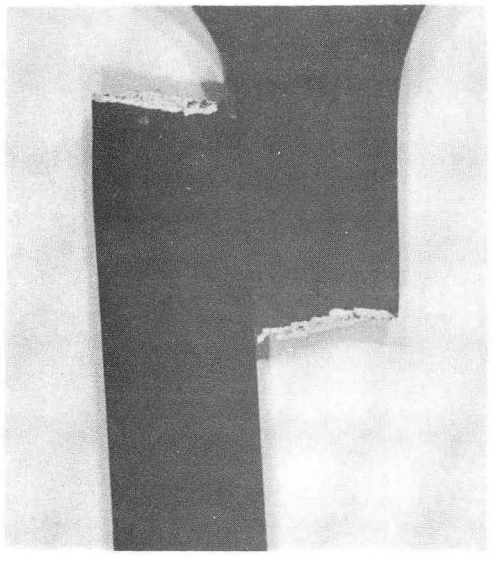

(a)

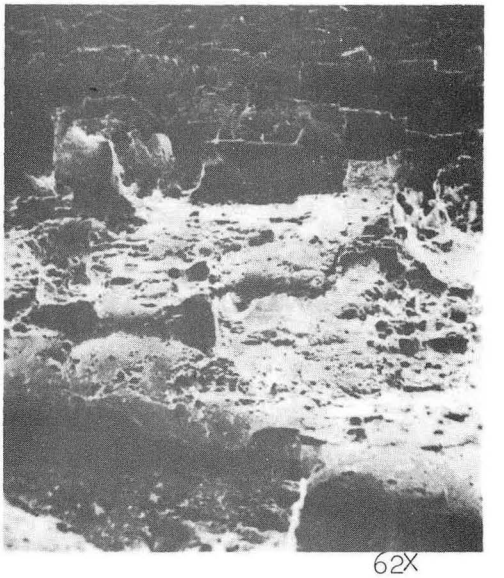

62X

(b)

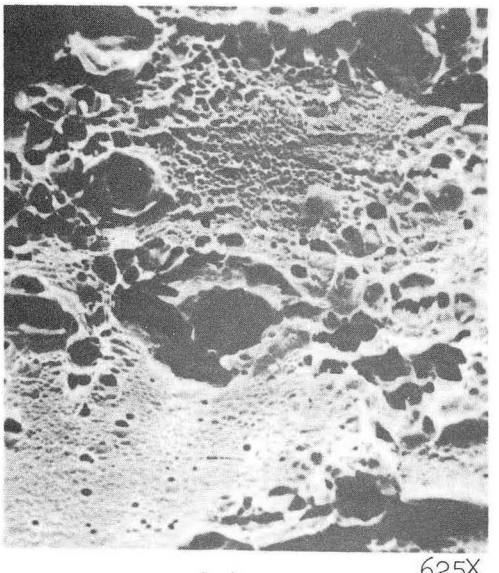

625X

(c)

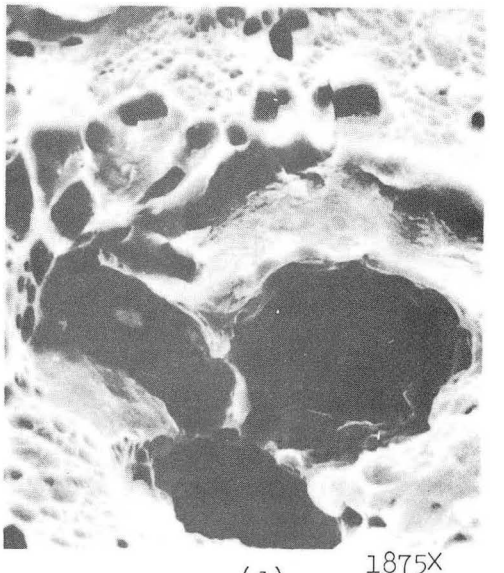

1875X

(d)

XBB 709-3957

Fig. 10

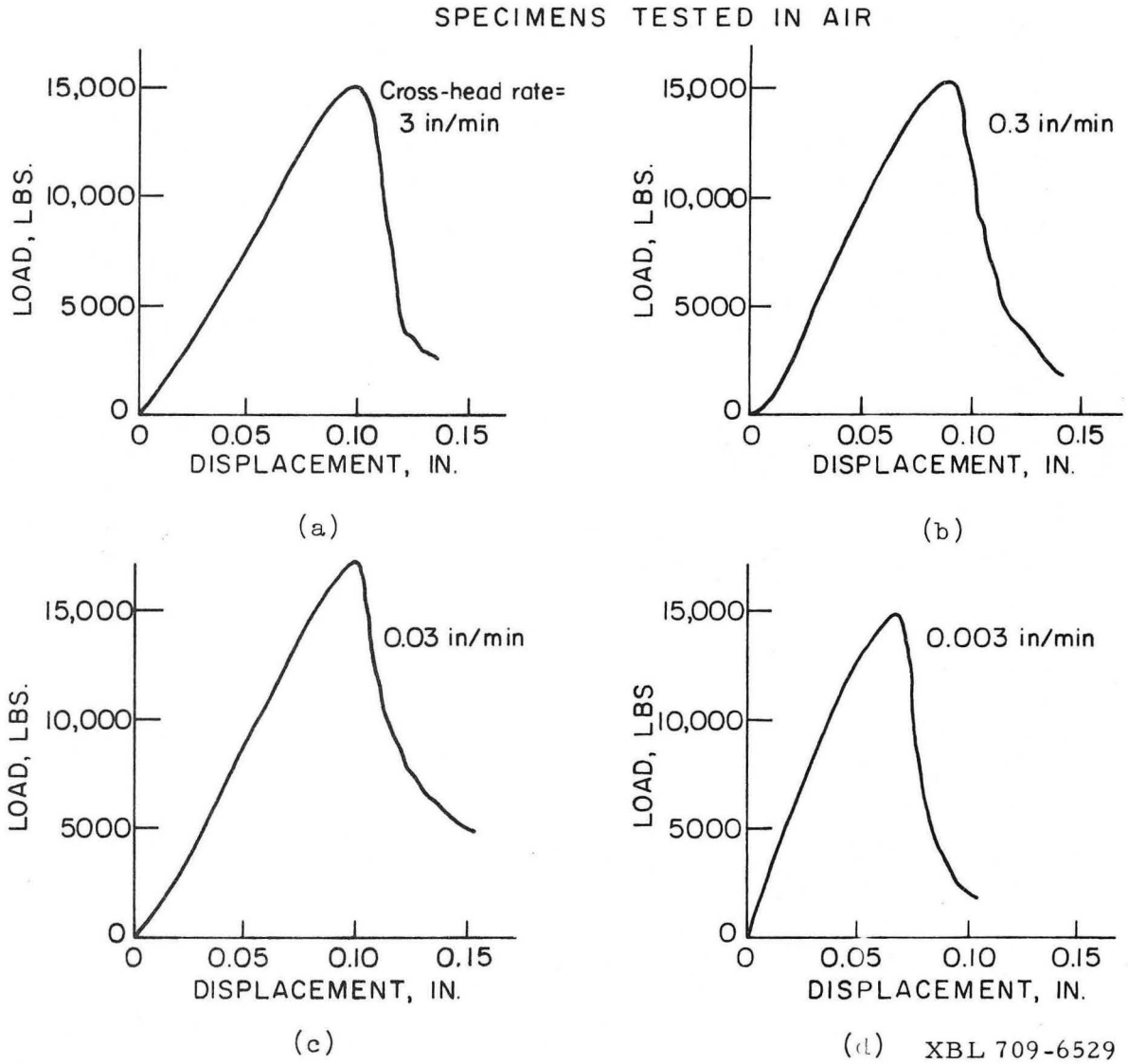
SPECIMENS TESTED IN AIR
15,000
10,000
5000
0
LOAD, LBS.
Cross-head rate=
3 in/min
0
0.05
0.10
0.15
DISPLACEMENT, IN.
(a)
0.3 in/min
(b)
0.03 in/min
(c)
0.003 in/min
(d)
XBL 709-6529

Fig. 4

SPECIMENS TESTED IN DISTILLED WATER

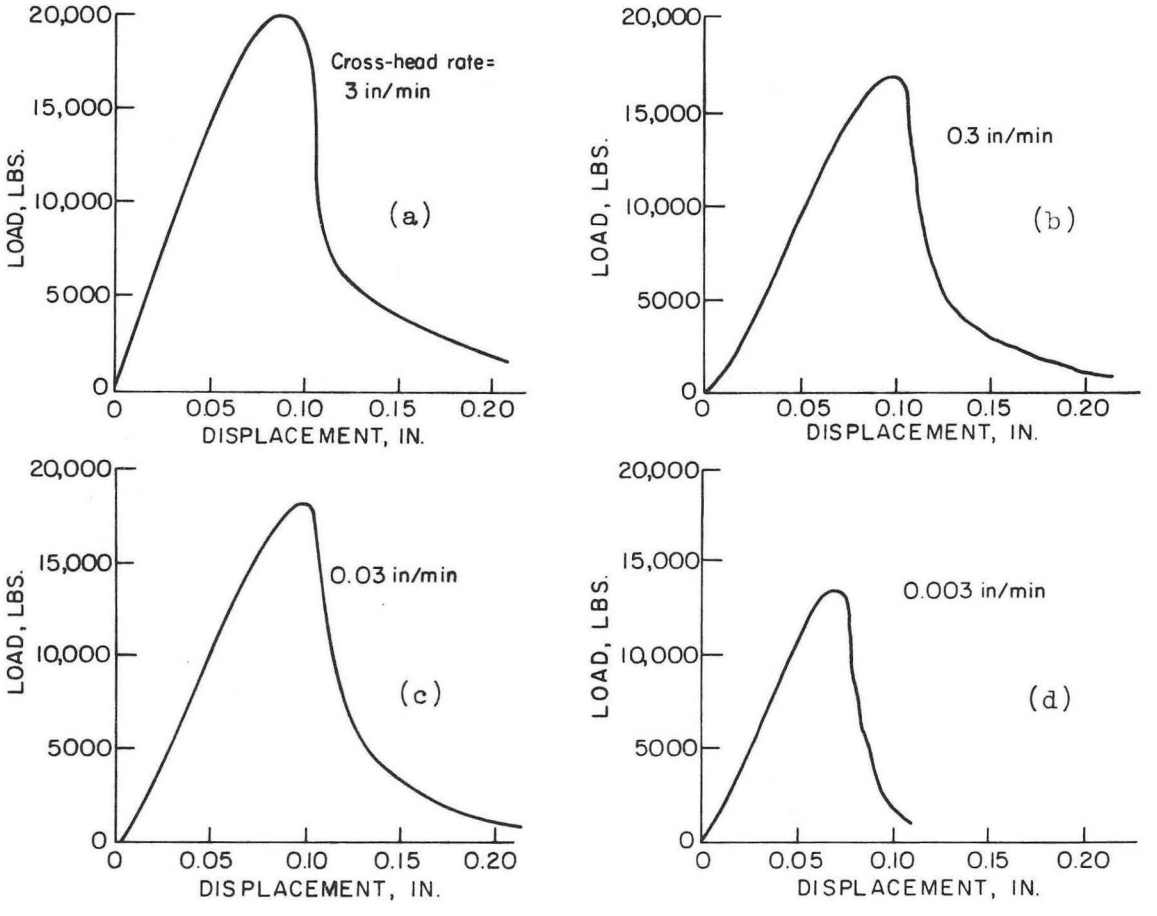

XBL 709-6530

Fig. 12

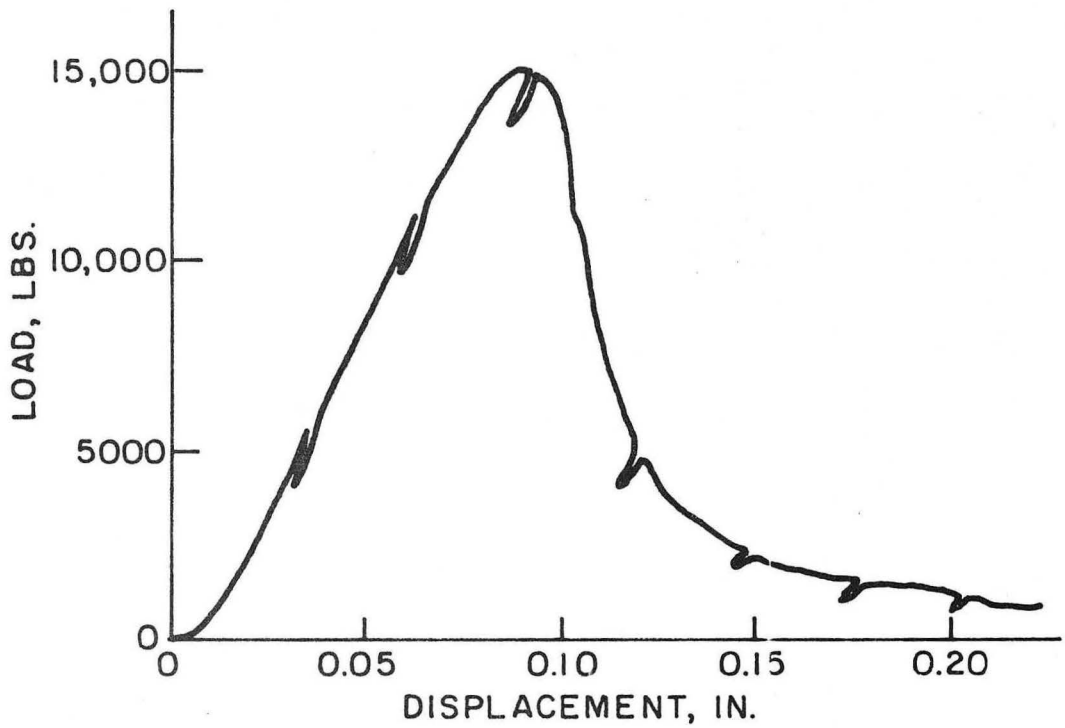

XBL 709-6521

Fig. 13

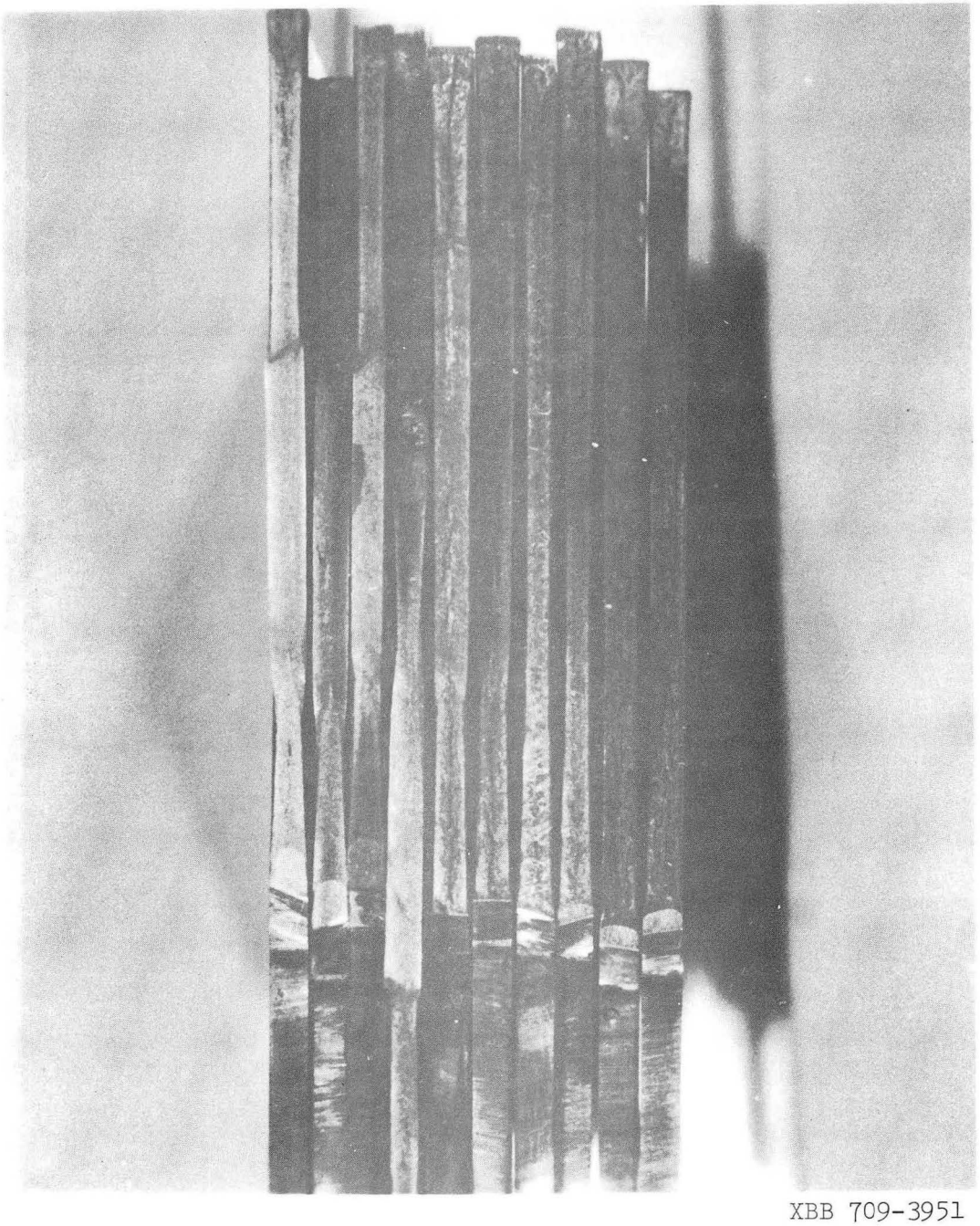

XBB 709-3951

Fig. 14

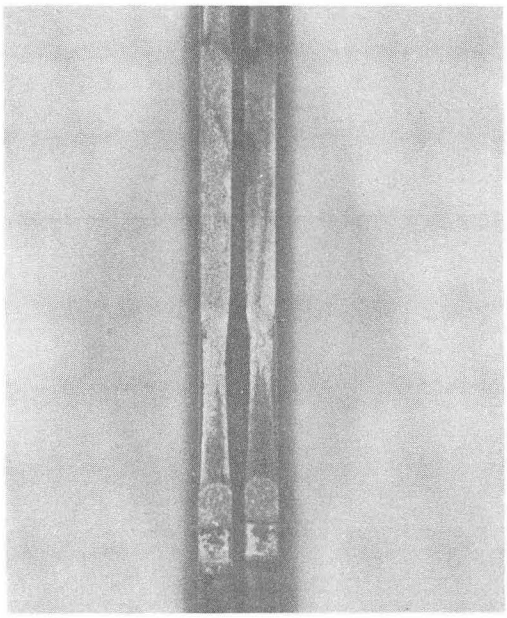

(a)

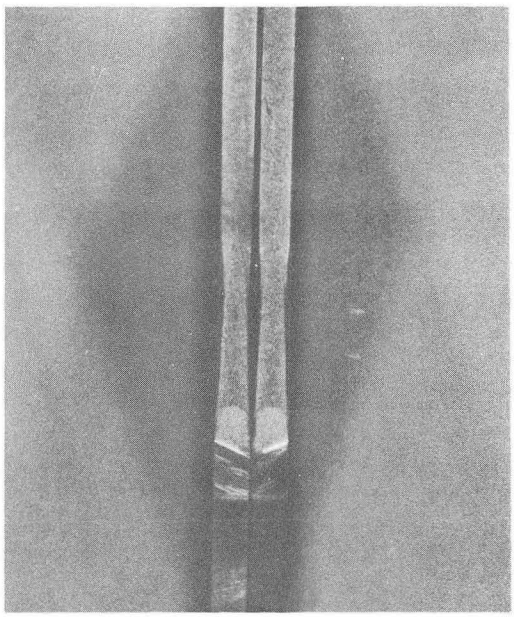

(b)

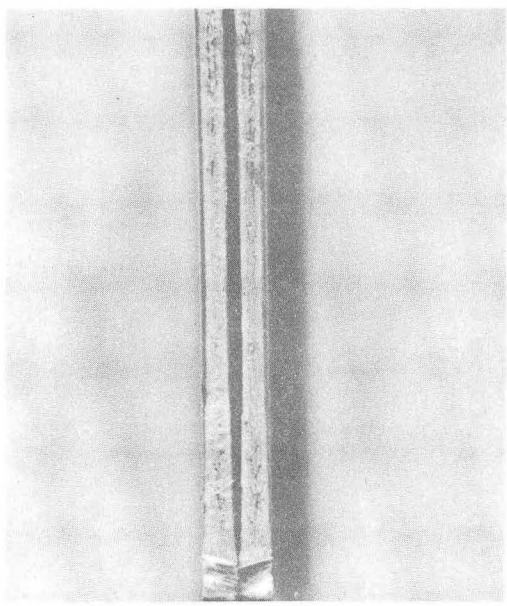

(c)

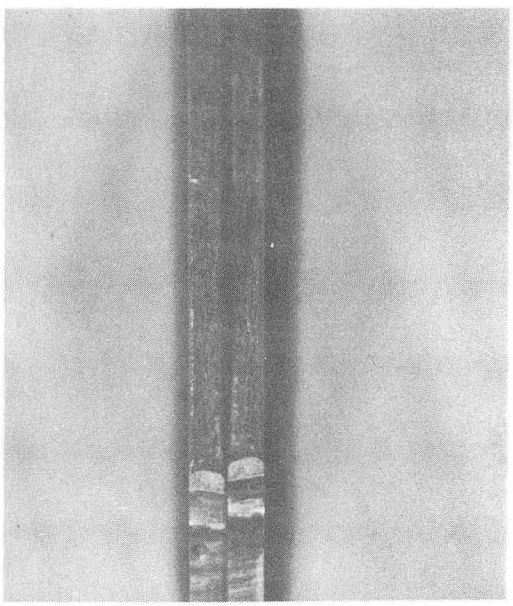

(d)

XBB 709-3953

Fig. 15

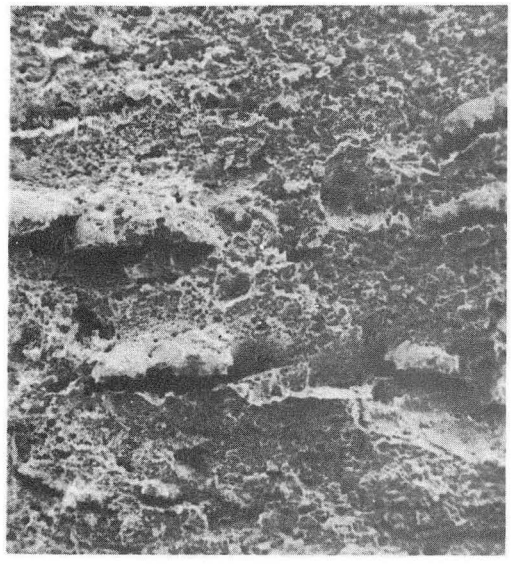

(a)

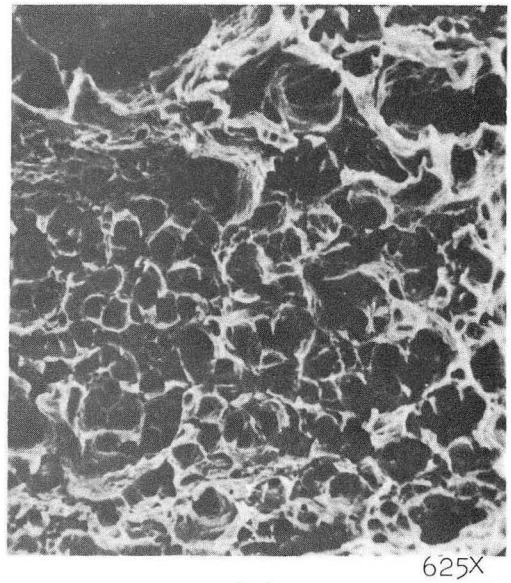

625X

(b)

6250X

(c)

XBB 709--3956

Fig. 16

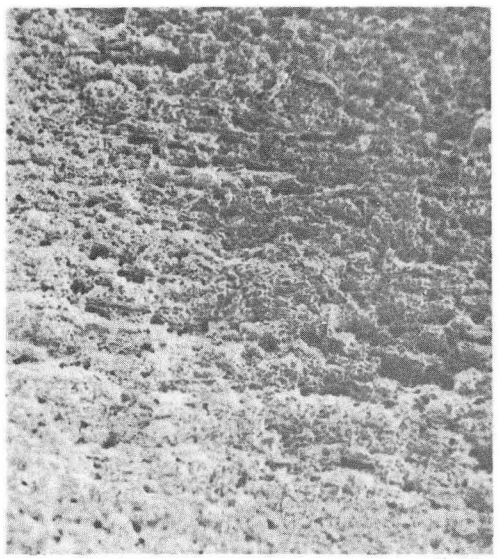

(a) 62X

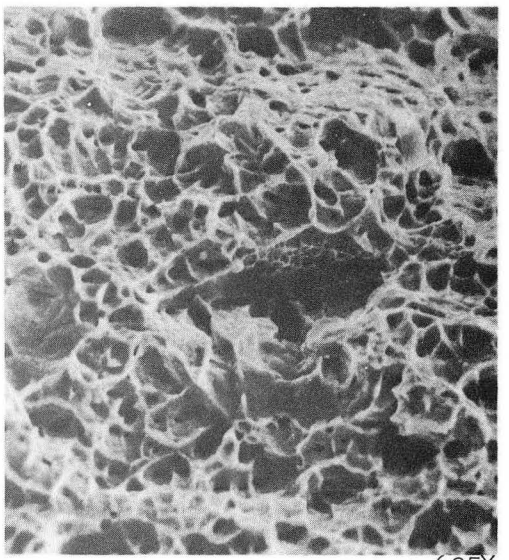

(b) 625X

6250X

(c)

XBB 709-3955

Fig. 17

62X

(a)

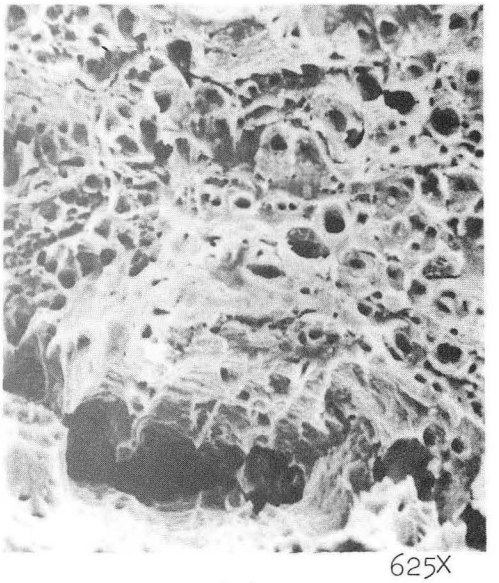

625X

(b)

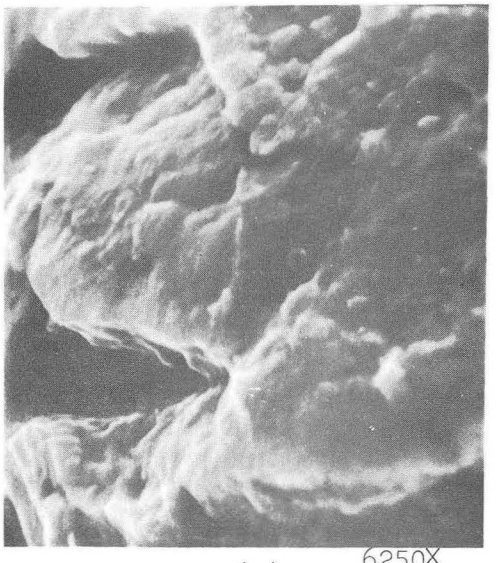

6250X

(c)

XBB 709-3959

Fig. 18

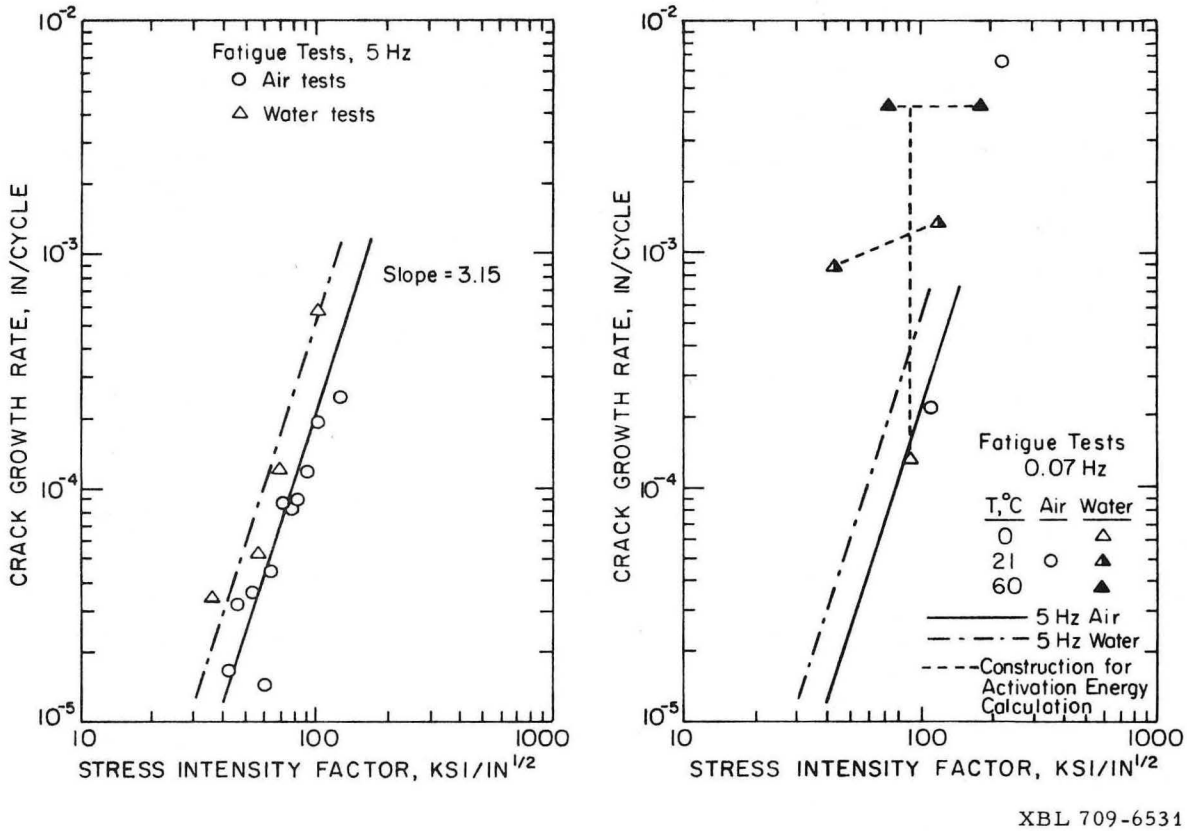
Fatigue Tests, 5 Hz
Air tests
Water tests
Slope = 3.15
CRACK GROWTH RATE, IN/CYCLE
STRESS INTENSITY FACTOR, KSI/IN^1/2
Fatigue Tests
0.07 Hz
T,°C Air Water
0
21
60
5 Hz Air
5 Hz Water
Construction for Activation Energy Calculation
XBL 709-6531

(a) (b)

Fig. 19

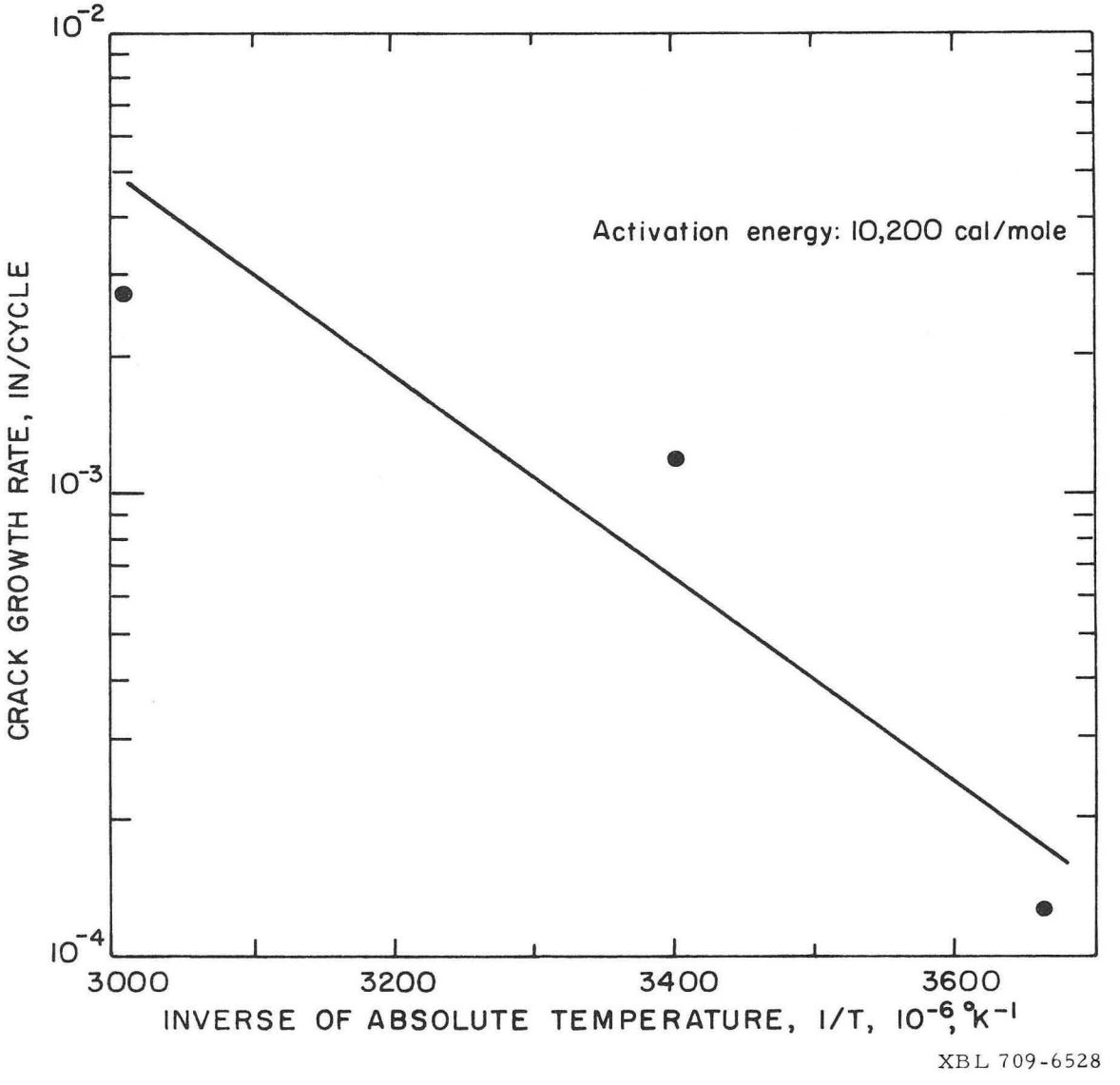
10^{-2}
10^{-3}
10^{-4}
CRACK GROWTH RATE, IN/CYCLE
Activation energy: 10,200 cal/mole
3000
3200
3400
3600
INVERSE OF ABSOLUTE TEMPERATURE, 1/T, 10^{-6}, °K^{-1}
XBL 709-6528

Fig. 20

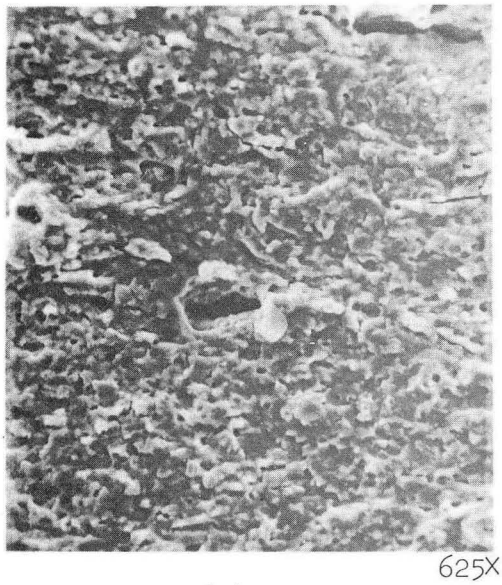

625X

(a)

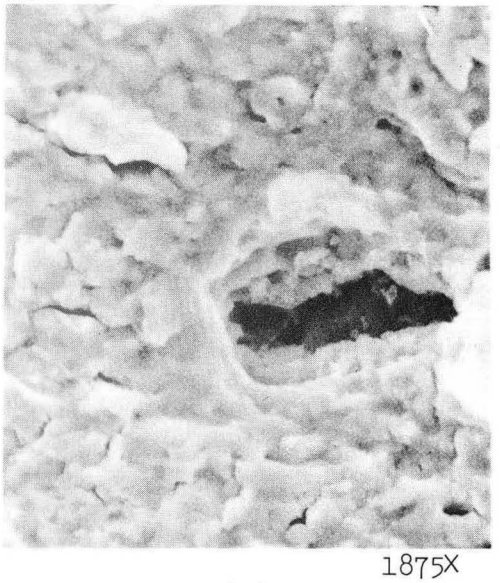

1875X

(b)

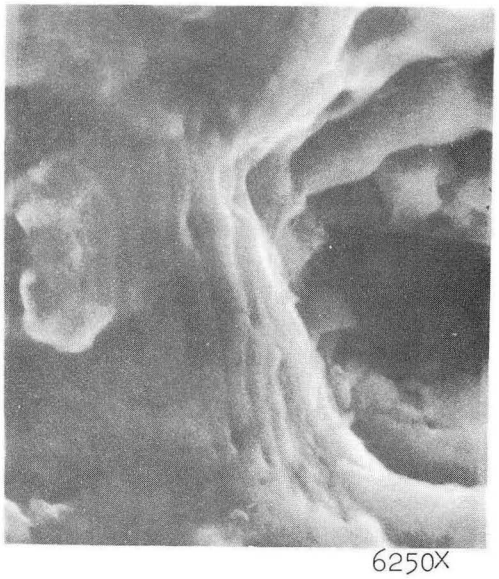

6250X

(c)

XBB 709-3960

Fig. 21

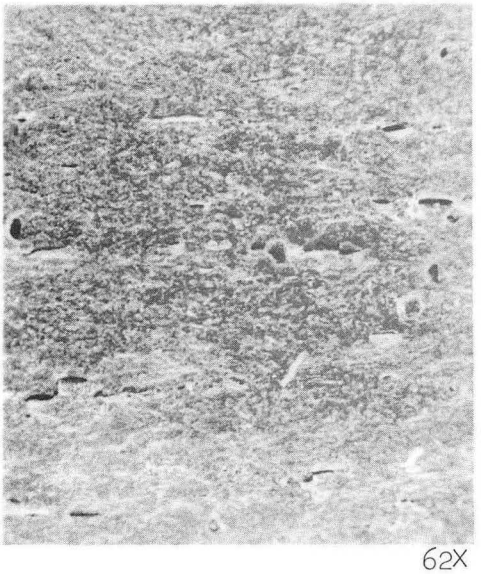

62X

(a)

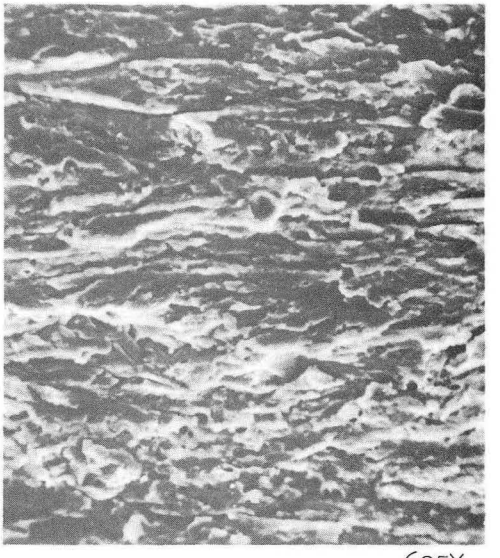

625X

(b)

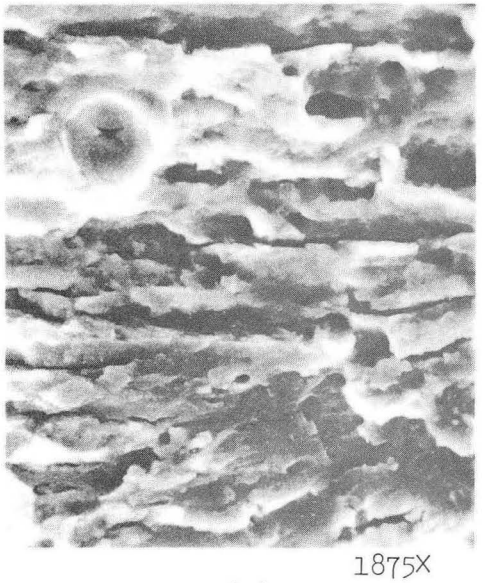

1875X

(c)

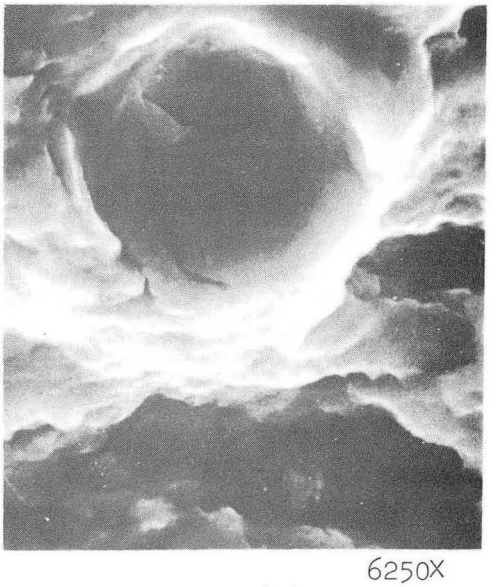

6250X

(d)

XBB 709-3954

Fig. 22

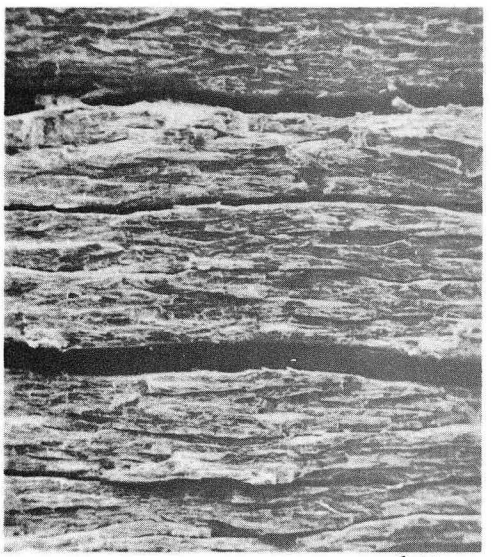

62X

(a)

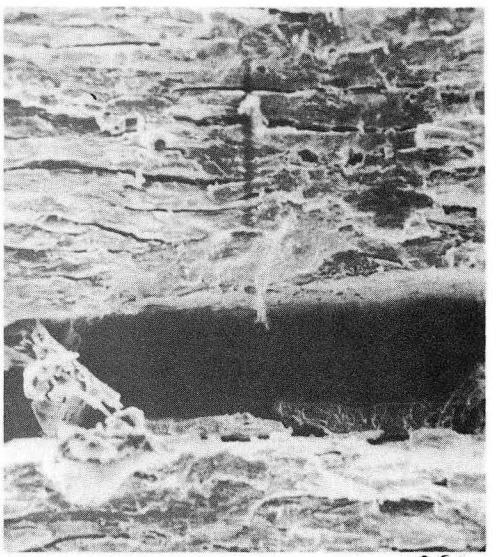

786X

(b)

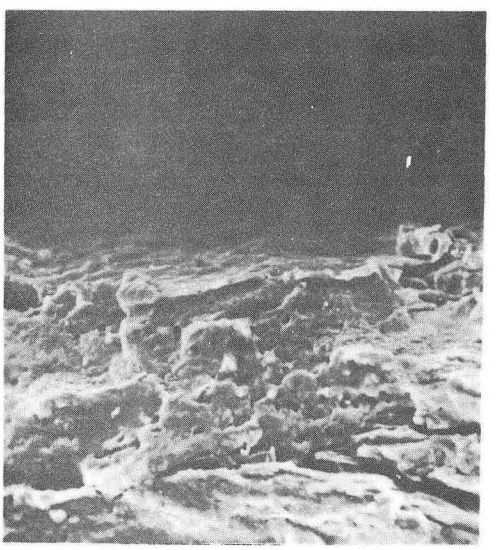

625X

(c)

XBB 709-3958

Fig. 23

(a)

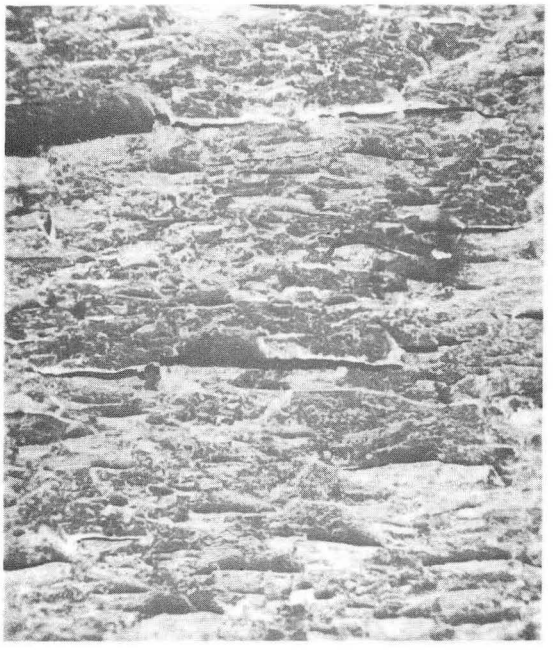

73X

(b)

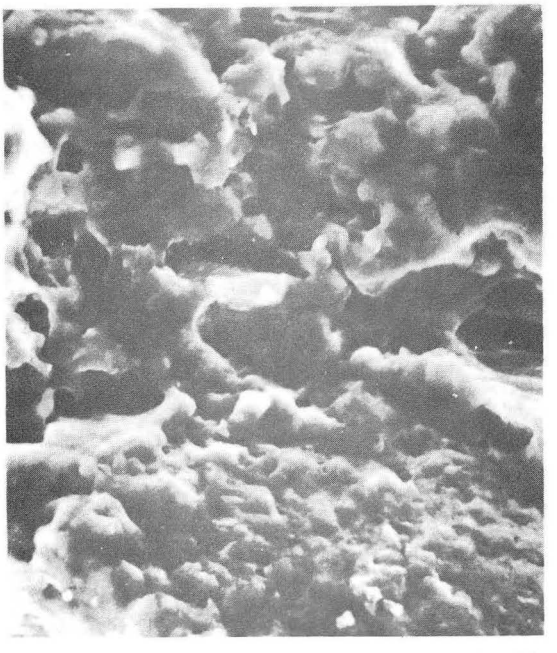

219X

XBB 709-3952

Fig. 24

124X

(a)

1240X

(b)

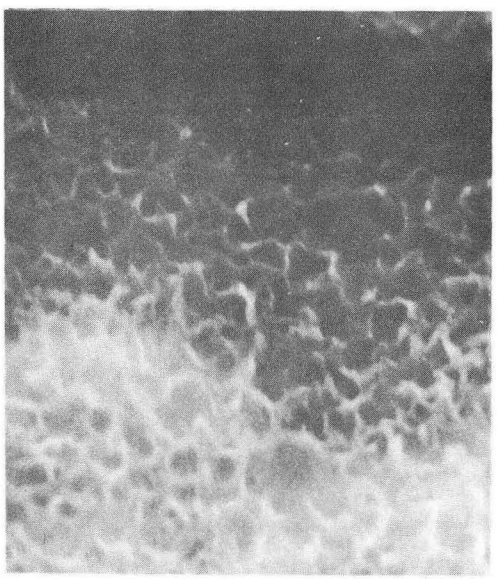

12,400X

(c)

XBB 709-3949

Fig. 25

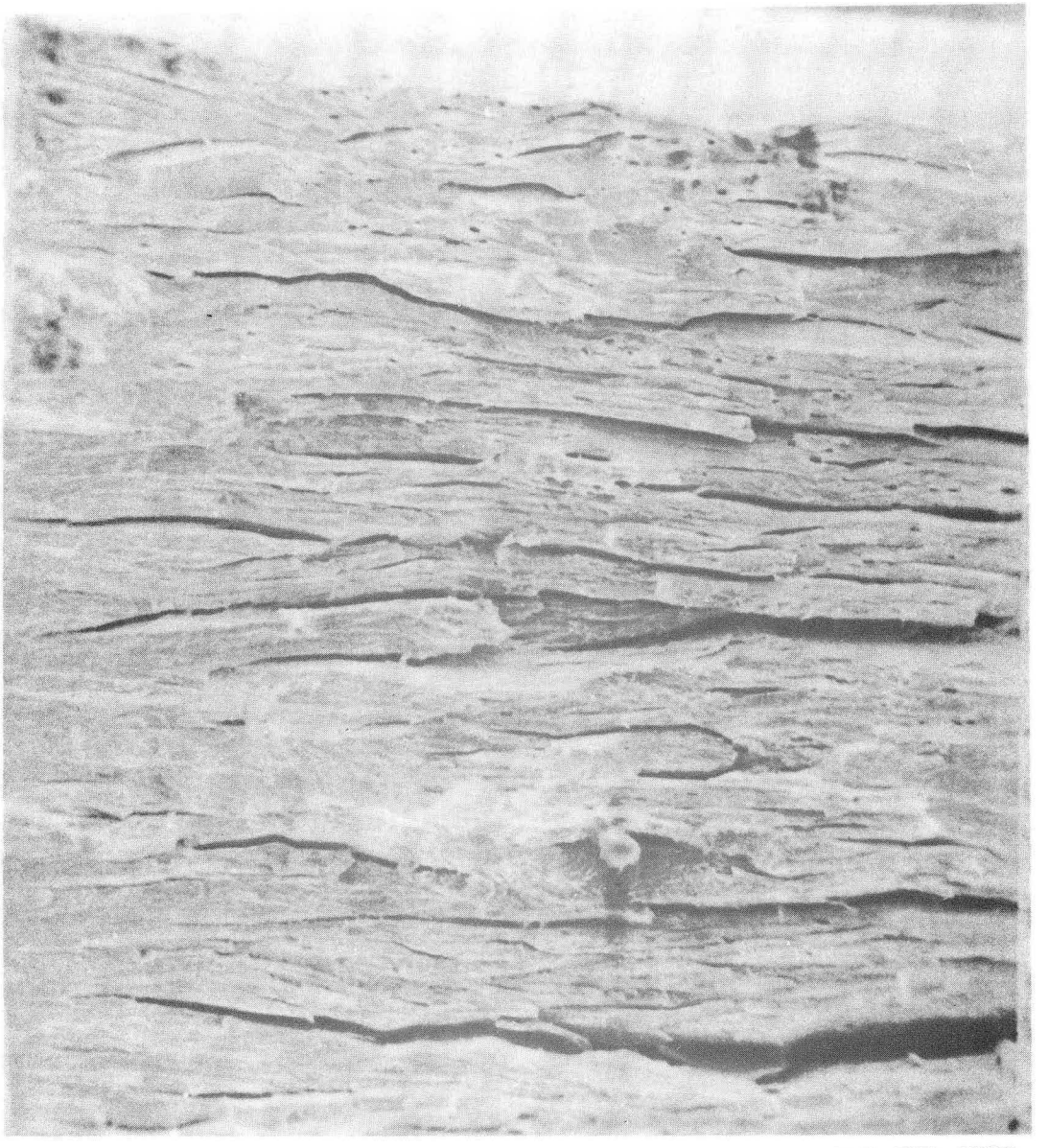

XBB 709-3950

Fig. 26

LEGAL NOTICE

This report was prepared as an account of Government sponsored work. Neither the United States, nor the Commission, nor any person acting on behalf of the Commission:

A. Makes any warranty or representation, expressed or implied, with respect to the accuracy, completeness, or usefulness of the information contained in this report, or that the use of any information, apparatus, method, or process disclosed in this report may not infringe privately owned rights; or

B. Assumes any liabilities with respect to the use of, or for damages resulting from the use of any information, apparatus, method, or process disclosed in this report.

As used in the above, "person acting on behalf of the Commission" includes any employee or contractor of the Commission, or employee of such contractor, to the extent that such employee or contractor of the Commission, or employee of such contractor prepares, disseminates, or provides access to, any information pursuant to his employment or contract with the Commission, or his employment with such contractor.

TECHNICAL INFORMATION DIVISION
LAWRENCE RADIATION LABORATORY
UNIVERSITY OF CALIFORNIA
BERKELEY, CALIFORNIA 94720